Peer-reviewed version available at Cancers 2020, 12, 881; doi:10.3390/cancers12040881

Extracellular Oncosomes Rich in Moonlighting Metalloproteinase (MMP3) Are Transmissive, Pro-Tumorigenic, and Induces Cellular Communication Network Factor 2 (CCN2/CTGF): CRISPR against Cancer

Yuka Okusha[1,2], Takanori Eguchi[1,3,*], Manh Tien Tran[1], Chiharu Sogawa[1], Kaya Yoshida[4], Mami Itagaki[1,5], Eman Ahmed Taha[1,6,7], Kisho Ono[8], Eriko Aoyama[3], Hirohiko Okamura[9], Ken-ichi Kozaki[1], Stuart K. Calderwood[2], Masaharu Takigawa[3], Kuniaki Okamoto[1]

[1] Department of Dental Pharmacology, Graduate School of Medicine, Dentistry and Pharmaceutical Sciences, Okayama University, Okayama, 700-8525, Japan.

[2] Division of Molecular and Cellular Biology, Department of Radiation Oncology, Beth Israel Deaconess Medical Center, Harvard Medical School, Boston, MA 02115, USA.

[3] Advanced Research Center for Oral and Craniofacial Sciences, Graduate School of Medicine, Dentistry and Pharmaceutical Sciences, Okayama University, Okayama, 700-8525, Japan.

[4] Department of Oral Healthcare Education, Institute of Biomedical Sciences, Tokushima University Graduate School, Tokushima, 770-8504, Japan.

[5] Research program for undergraduate students, Okayama University Dental School, Okayama 700-8525, Japan.

[6] Department of Medical Bioengineering, Graduate School of Natural Science and Technology, Okayama University, Okayama 700-8530, Japan.

[7] Department of Biochemistry, Ain Shams University Faculty of Science, Cairo 11566 Egypt.

[8] Department of Oral and Maxillofacial Surgery, Okayama University Hospital, Okayama 700-0914 Japan.

[9] Department of Oral Morphology, Dentistry and Pharmaceutical Sciences, Okayama University Graduate School of Medicine, Okayama, 700-8525, Japan.

*To whom correspondence should be addressed:

Takanori Eguchi, DDS, PhD

2-5-1, Shikata-cho, Kita-ku, Okayama city, 700-8525, Japan

Tel: +81-86-235-6662; Fax: +81-86-235-6664

Email: eguchi@okayama-u.ac.jp

eguchi.takanori@gmail.com

Short title: Oncosomal delivery of MMP3 trans-activating CCN2

Abstract

Within the tumour microenvironment, extracellular vesicles (EVs) mediate intercellular communication and the exchange of biomolecules between cells. Matrix metalloproteinase 3 (MMP3) plays multiple roles in pro-tumorigenic proteolysis and in intracellular transcription. These include inducing connective tissue growth factor [CTGF, also known as cellular communication network factor 2 (CCN2)] and prompting a new definition of MMP3 as a moonlighting metalloproteinase. Members of the MMP family have been found within tumor-derived EVs such as oncosomes or exosomes. We here investigated the roles of MMP3-rich oncosomes in tumor progression, molecular transmission, and gene regulation. MMP3 and CCN2/CTGF were significantly co-expressed in tumor samples derived from patients suffering from colorectal adenocarcinoma. We found that oncosomes derived from a rapidly metastatic cancer cells were enriched in MMP3 and a C-terminal half fragment of CCN2/CTGF. MMP3-rich oncosomes were highly transmissive into recipient cells and pro-tumorigenic in an allograft mouse model. Oncosome-derived MMP3 was transmissive into recipient cell nuclei, trans-activated CCN2/CTGF promoter, and induced CCN2/CTGF production at 1 to 6 hours after the addition of oncosomes to culture media. In addition, CRISPR/Cas9-mediated knockout of MMP3 showed significant anti-tumor effects, including inhibition of migration and invasion of tumor cells in vitro, inhibition of tumor growth in vivo, and reduction of CCN2/CTGF and its promoter activity in vitro. These data newly demonstrate that the oncosome-derived moonlighting metalloproteinase promotes metastasis and is pro-tumorigenic at distant sites as well as a transmissive trans-activator for the cellular communication network gene.

Keywords: matrix metalloproteinase (MMP); moonlighting metalloproteinase; extracellular vesicles; oncosome; genome editing; cellular communication network factor 2 (CCN2/CTGF); transcription factor; cancer

Peer-reviewed version available at Cancers 2020, 12, 881; doi:10.3390/cancers12040881

1. Introduction

Cancer is one of the most common causes of death, lethalty involving metastasis and therapy resistance. Poor prognosis in cancer patients is associated with rapid tumor progression, tumor-stroma interactive microenvironment, the dissemination of tumor cells from a primary lesion to the blood circulation and escape to distant organs where metastatic secondary tumors are formed [1,2]. Recent studies have shown that extracellular vesicles (EVs) released from the cells can transfer bioactive molecules to the neighboring cells and deliver to distant organs through body fluids such as the bloodstream. EV-mediated molecular transfer is essential for a number of events in tumor progression, including epithelial-mesenchymal transition (EMT), tumor-stroma interaction, and metastasis [3-5]. EVs can promote the dissemination of cancer cells through body fluids [6], the formation of pre-/pro-metastatic niche [7], and education of myeloid cells [8]. Tumor EVs often contain oncogenic proteins such as heat shock proteins (HSP), CD326/EpCAM, EGFR, EGFRvIII, and KIT [3,9-14]. It has been shown that the molecular transfer of oncogenic proteins is able to transform recipient cells, such as EMT [3,9], prompting to use the term "oncosome" suggesting the oncogenic properties of tumor-derived vesicles. Notably, a number of EV proteins are common with protein secretome, including matrix metalloproteinases (MMP) and cellular communication network factors (CCN family proteins) [15]. In the present study, we aimed to investigate a mechanism of how oncosomal MMP3 promotes tumor progression in vitro and in vivo.

It has been shown that MMP3 and CCN2 (also known as CTGF named after connective tissue growth factor) are often increased in tumor-stroma tissues or patient serum and are thus biomarkers correlated with poor prognosis in cancer [16-20]. It has been also shown that MMP3 and CTGF promote tumor progression including rapid metastasis and tumor-stroma interactions [21-24]. CTGF up-regulates MMP family proteins in cancer [25], whereas MMP3 regulates CCN2/CTGF by two mechanisms, including: (i) intracellular MMP3 directly activate the *CCN2/CTGF* gene to induce production of CCN2/CTGF protein in chondrocytes [26,27], (ii) MMPs directly cleave CCN2/CTGF to generate bioactive fragments essential for angiogenesis and osteoclastogenesis [28,29]. However, it had not been investigated whether / how MMP3 could control CCN2/CTGF in cancer, a process which we aimed to examine, in the current study.

Previously we focused on mechanisms underlying the robust expression of CCN2/CTGF in connective tissues such as cartilage and in tumors [30,31]. Promoter analysis of CCN2/CTGF revealed a cis-element designated transcriptional enhancer dominant in chondrocytes (TRENDIC) [32]. One of the TRENDIC-binding proteins was identified to be MMP3. MMP3 overexpression enhanced CTGF promoter activities in human chondrosarcoma-derived chondrocytic cell line HCS-2/8 and non-basal type, triple-negative breast cancer cell line MDA-MB-231 [26]. Intranuclear translocation of recombinant MMP3, as well as endogenous MMP3, was

observed under confocal laser scanning microscopy (CLSM) [26]. DNA-binding of MMP3 was next demonstrated by gel shift and chromatin immunoprecipitation assays. Human MMP3 also contains six basic amino acid clusters, which were shown to be nuclear localization signals (NLS) [27]. An MMP3 specific inhibitor inhibited the activity of the CTGF promoter, suggesting that MMP3 proteolytic activity was required for the transcriptional role for this enzyme, although general MMP inhibitor GM6001 or an MMP2/9 inhibitor were each ineffective in HSC-2/8 cells [26]. MMP3 was immunostained in cell nuclei in cartilage tissues in the normal and arthritic mouse model. However, vesicle-associated transport and roles of MMP3 in cancer have not been unveiled, a mechanism which we aimed to investigate here.

In addition we have recently developed an allograftable metastatic tumor model in mice [21,33]. A colon cancer cell line Colon26 was generated from a BALB/c mouse and a rapidly metastatic cancer cell line LuM1 was then generated by the inoculation of Colon26 into mice and repetitive metastasis experiments [34]. Notably, the LuM1 cells expressed MMP3 and MMP9 at high levels compared to Colon26. RNA interference (RNAi) targeting MMP3 or MMP9 significantly lowered tumor growth and metastasis in the allograft mouse model [21]. In the present study, we generated MMP3-knockout (MMP3-KO) cells, by using CRISPR-Cas9 genome editing technology on the LuM1 cells and compared the oncogenic effects of these cells and their derived vesicles. We also have shown that MMP3 was distributed at the tumor-stroma border area and immunostained in cell nuclei in a tumor allograft mouse model [21]. We therefore hypothesized that molecular transmission of MMP3 during the tumor-stroma interaction could underlie the pro-tumorigenic and pro-metastatic roles of this multi-functional proteinase, and we also aimed to investigate this mechanism in the present study.

2. RESULTS

2.1. Metastatic cancer-derived, MMP3-rich oncosomes are highly transmissive.

To characterize the properties of high metastatic LuM1-derived oncosomes, we prepared EVs from the culture supernatants of Colon26 and LuM1 cells and then analyzed their morphology and transmissive and pro-tumorigenic potentials. Vesicular structures with a cup-shaped morphology sized between 50 and 200 nm were found in the EV fractions of both Colon26 and LuM1 cells under TEM (Fig. 1A). Particle diameter distribution analysis revealed that both cell types secreted EVs (50 to 400 nm) with single peaks at approx. 150 nm (Fig. 1B). These data indicated that both LuM1 and Colon26 cells secrete heterogeneous EVs including exosomes and ectosomes.

We next examined whether MMP3 was contained in the EVs and non-vesicular extracellular fractions of LuM1 and Colon26 cells. The anti-MMP3 C-terminus antibody detected full-length MMP3 at markedly higher levels in the cell lysate, EV fraction and non-EV fraction of LuM1 cells (Fig. 1C, arrowheads; Fig. S1). Notably,

Preprints (www.preprints.org) | NOT PEER-REVIEWED | Posted: 19 February 2020 doi:10.20944/preprints202002.0281.v1

Peer-reviewed version available at Cancers 2020, 12, 881; doi:10.3390/cancers12040881

the same anti-MMP3 antibody detected the C-terminal PEX fragment of MMP3 in LuM1-EV fraction, suggesting that active metalloproteinases could self-cleave MMP3 in/on the oncosomes (Fig. 1C, arrows).

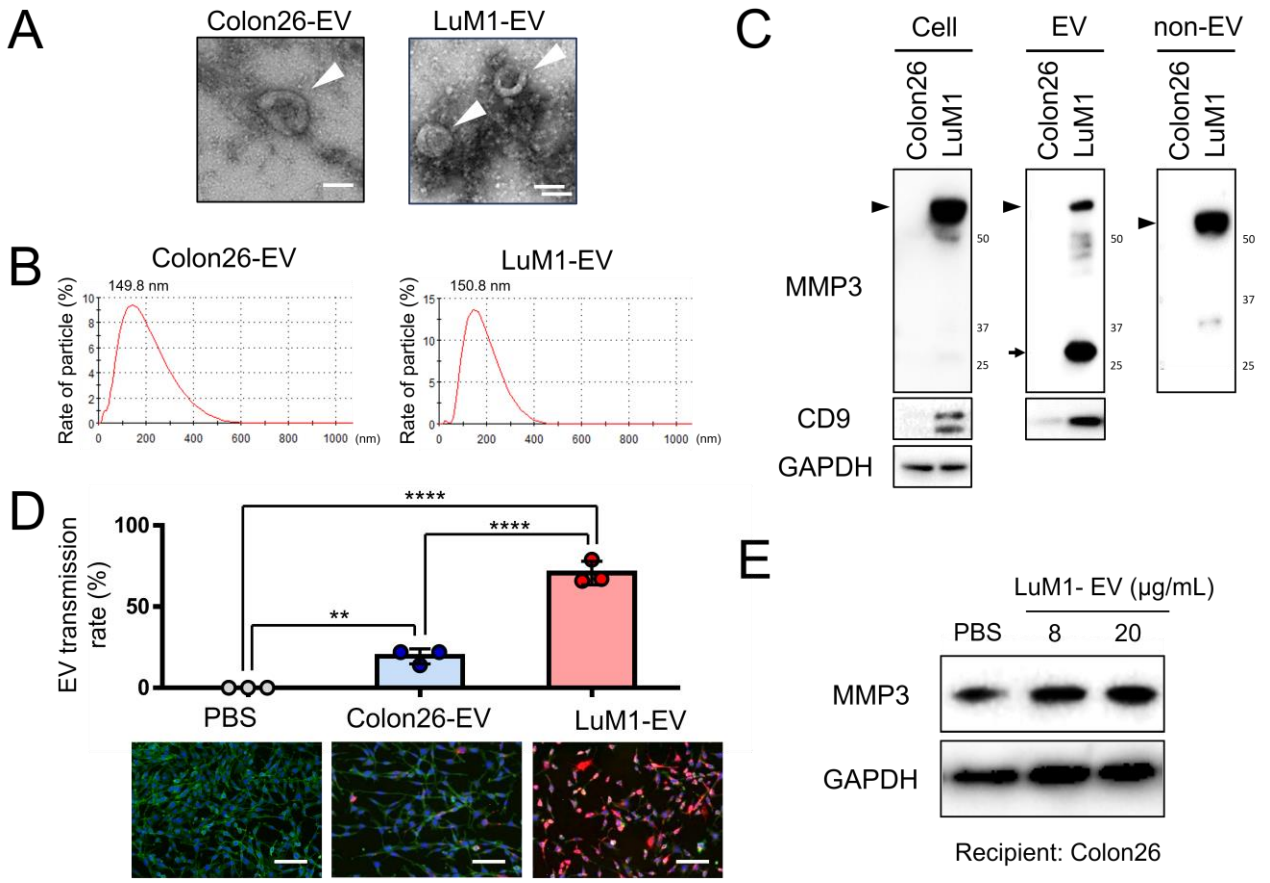

Fig. 1 | Metastatic cancer-derived, MMP3-rich oncosomes are highly transmissive. Roles of EVs derived from low-metastatic Colon26 cells vs. high-metastatic LuM1 cells were compared. (A) Representative TEM images of EVs. Arrowheads indicate EVs with cup-shaped morphology. Scale bars, 100 nm. (B) Particle diameter distribution of EV fractions. (C) Western blot analysis of MMP3 and CD9 in cell lysates, EV and non-EV fractions. Arrowhead indicates full-length MMP3 (54 kDa). Arrows indicate the 25-kDa PEX isoform of MMP3. (D) Transmission efficiencies of EVs. EVs were labeled with red fluorescent ceramide and added to culture media of the recipient Colon26 cells at a final concentration of 11.5 μg/mL for 24 hours. Cells were fixed and stained with ActinGreen and DAPI. Top, EV transmission efficiencies. The efficiencies were the ratio of transmitted EV-positive cells to the total number of cells. **p<0.01, ****p<0.0001, n=3 fields. Bottom, representative images of EV transmission. Scale bars, 100 μm. (E) Western blot showing a potential molecular transfer of MMP3. LuM1-EVs (8 or 20 μg/mL) enriched with MMP3 were added to culture media of the recipient Colon26 cells (MMP3 low) for 9 h. The experiments were repeated twice in Fig 1C, E.

CD9, an established marker of exosomes, was also detected in LuM1-EVs and cell lysate at higher levels than in Colon26, suggesting that LuM1 produced CD9/MMP3-oncosomes while Colon26 produced other types of vesicles (Fig. 1C). We next examined whether transmissive potentials of oncosomes could be different between LuM1- and Colon26-derived EVs. LuM1-derived EVs were more activively transmitted into the

recipient cells compared to Colon26-derived EVs (Fig. 1D), suggesting that LuM1-EVs may promote more endosomal escape than Colon26-EVs. Furthermore, the MMP3 levels in the recipient Colon26 cells were markedly increased upon the addition of the MMP3-rich LuM1-EVs (Fig. 1E, Fig. S2), suggesting that MMP3 in/on the EVs was transferred to the recipient cells.

These experiments indicated that the MMP3-rich oncosomes released by the more aggressive cancer cells were highly transmissive into the recipient cells.

2.2. The pro-tumorigenic effects of oncosomes in vivo.

To investigate the functions of LuM1-oncosomes in cancer progression, we next examined whether intraperitoneally injected LuM1-oncosomes could alter the subcutaneously allografted tumors through body fluid in mice. Indeed, LuM1-oncosomes significantly promoted tumor growth as compared to the PBS-injected control group and to the Colon26-EV group (Fig. 2 A, B, C). Bodyweight of mice was more increased in tumor/Colon26-EV injection group as compared to the tumor/PBS-injected group. On the other hand, bodyweight loss in mice was seen by the injection of the LuM1-EVs, suggesting that cachexia might be caused by the LuM1-derived oncosomes (Fig. 2D). In order to monitor the organ-tropic transmission of EVs, we next labeled EVs with Cy7 fluorescent dye which was intraperitoneally injected into mice and then visualized using an in vivo imaging system. LuM1-EVs distributed to the lung, where Colon26-EVs were undetectable (Fig. 2E), consistent with the lung-tropic metastatic property of LuM1 cells. LuM1-EVs also distributed to the head, where Colon26-EVs were undetectable. Both LuM1-EVs and Colon26-EVs primarily distributed to the livers.

These data indicate that MMP3-rich oncosomes released by the aggressive cancer cells are highly transmissive to multiple organs, including lung, head, and liver, and pro-tumorigenic through the body fluids.

Preprints (www.preprints.org) | NOT PEER-REVIEWED | Posted: 19 February 2020 doi:10.20944/preprints202002.0281.v1

Peer-reviewed version available at Cancers 2020, 12, 881; doi:10.3390/cancers12040881

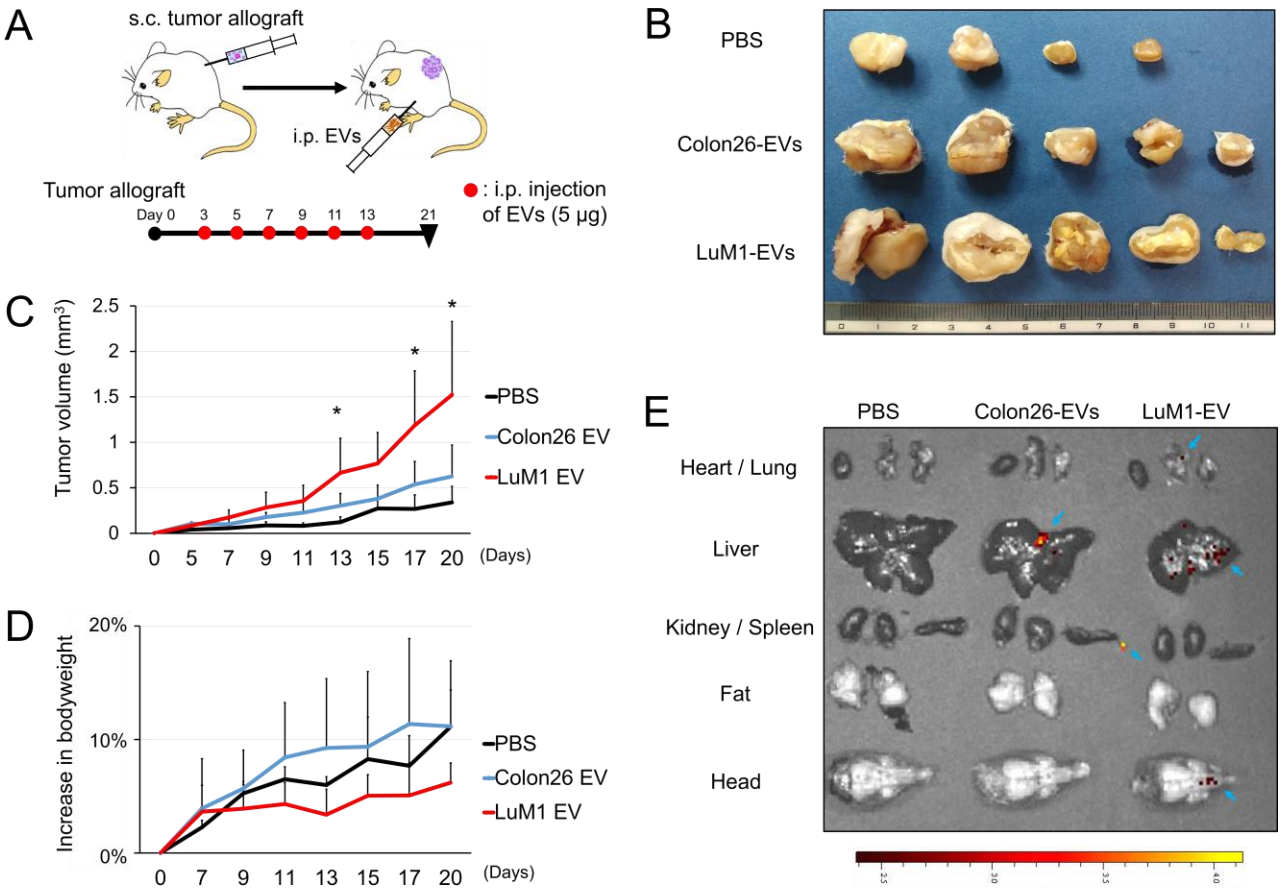

Fig. 2 | Pro-tumorigenic effects of oncosomes mediated through the body fluids. (A) A schema of the animal experiment. Colon26 cells were injected subcutaneously (s.c.) into the side abdominal wall of BALB/c mice at the volume of 5.0×10^5 cells/ 0.5 mL PBS. After the transplantation, Colon26 EV fraction, LuM1 EV fraction or PBS were injected intraperitoneally (i.p.) at the volume of 5 μg / 0.5 mL PBS from day 3 to day 13, every other day, 6 times. (B) Representative images of subcutaneous tumors on day 21 after i.p. (C, D) Tumor growth (C) and bodyweights (D) altered by exogenous EVs. PBS group, n=3; Colon26 EV group, n=4; LuM1 EV group, n=5. Mean+SD, *p<0.05 as compared with PBS group. D, the percentage increases in bodyweights to day 0 were plotted. (E) In vivo imaging of EV transmission. EVs were labeled with Cy7 and then injected intraperitoneally. In vivo images were taken 24 hours after the administration. The experiments were repeated twice each in Fig. 2A, B, C, D.

2.3. Establishment of MMP3 knockout cells using the CRISPR/Cas9 genome editing technology.

In order to establish MMP3-knockout cells, we next edited the genome of LuM1 cells. We found a targetable repetitive CRISPR sequence (5'-TGCA……TGCA-3') followed by a PAM sequence (5'-TGG -3') in the antisense strand in exon 1 of *Mmp3* gene (Fig. 3A). We designed and synthesized guide RNA (gRNA) targeting the CRISPR sequence and then transfected a ribonucleoprotein (RNP) complex composed of the gRNA and recombinant Cas9 (rCas9) nuclease using a transfection reagent. We first established three clones of mono-

allelic insertion or deletion (INDEL) in a total of 21 clones (Fig. 3B, Table 1, Fig. S3). Three types of mono-allelic INDEL clones were composed of two heterogenic deletion clones (clone #14 with 43-base deletion, clone #21 with 19-base deletion) and one heterogenic insertion clone (clone #11 with 16-base insertion).

Table 1. Genome editing efficiencies.

	First edit	Second edit
Method of Cas9/gRNA transfection	Reagent	Electroporation
The number of investigated clones	21	8
Mono-allelic INDEL	3	n.a.
Bi-allelic INDEL	n.a.	6
Changes in the number of nucleotides	+16, -43, -19	-1
Genome editing efficiency	14.3%	75%

n.a., not available

To establish a bi-allelic deletion clone, we secondly transfected the same RNP complex into clone #14 by using an electroporation-transfection method. By single-cell cloning, we establish eight clones, then prepared a bi-allelic deletion clone with additional single nucleotide deletion with 75% efficiency in the counterpart allele (Fig. 3 C, D, Table 1), suggesting that these bi-allelic deletions cause frame-shifts in exon 1 and the subsequent premature termination codon. To verify the knockout of MMP3, we then performed RT-qPCR and western blotting. The mRNA level of MMP3 in the bi-allelic deletion clone was significantly lower than that of LuM1 cells, suggesting that mutant mRNAs of MMP3 were barely transcribed and unstable (Fig. 3E). MMP3 protein was undetectable in the MMP3-KO cells while being detectable in LuM1 cells (Fig. 3F).

Preprints (www.preprints.org) | NOT PEER-REVIEWED | Posted: 19 February 2020 doi:10.20944/preprints202002.0281.v1

Peer-reviewed version available at Cancers 2020, 12, 881; doi:10.3390/cancers12040881

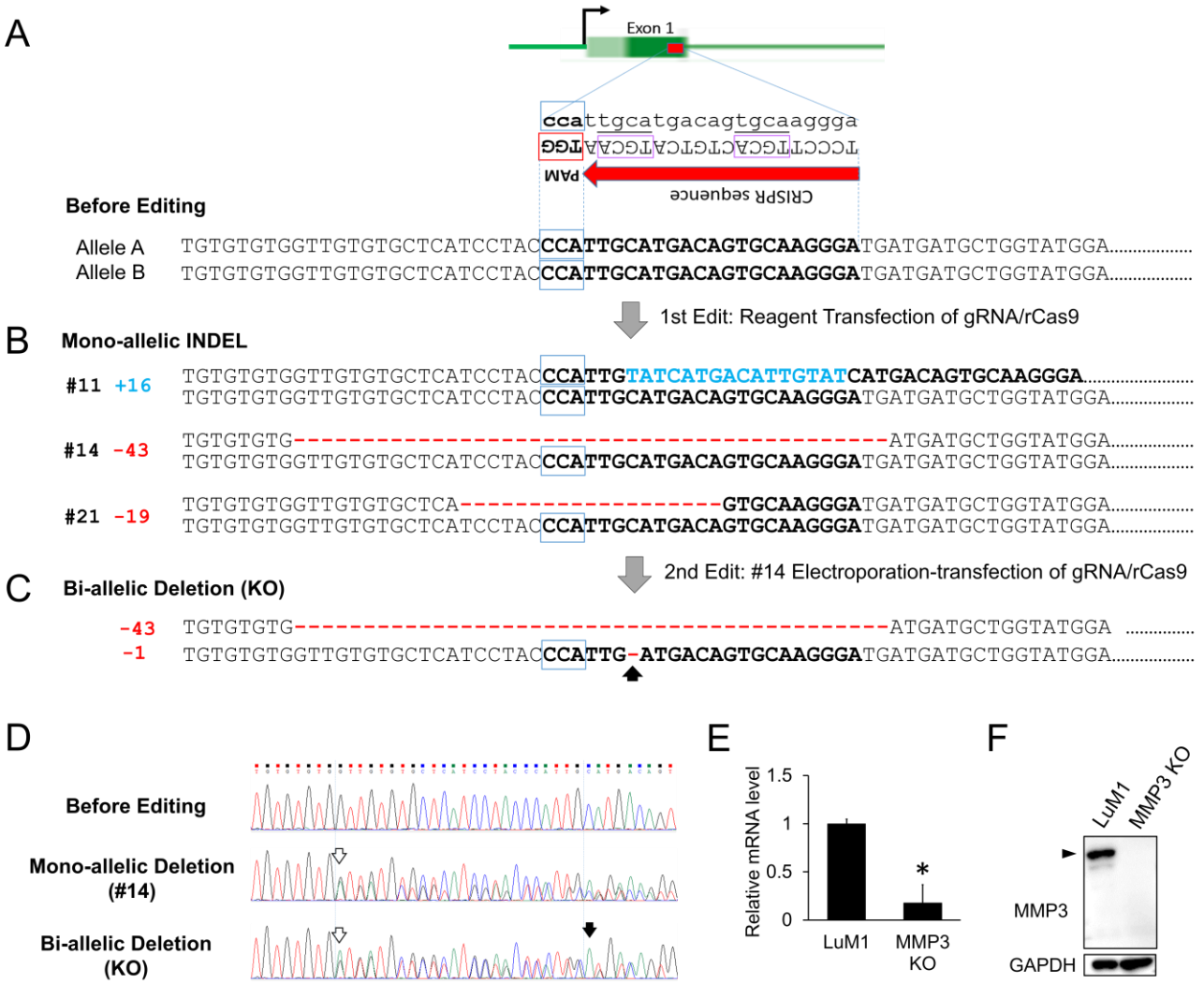

Fig. 3 | Establishment of MMP3 knockout cells using CRISPR/Cas9 genome editing technology. (A) Schemes representing targeting of exon 1 in MMP3 gene. Top, a scheme of MMP3 gene. Dark green box, a coding region of exon 1 including the target sequence. Bright green box, 5'-untranslated region. Middle, a CRISPR sequence containing 5'-TGCA-3' repeat enclosed with purple square, tailed with PAM sequence (TGG) in the antisense strand. Bottom, a partial sequence of MMP3 exon 1 including the target sequence (shown in bold). (B) The sequences of mono-allelic INDEL clones. Three types of mono-allelic INDEL clones were obtained. Clone #11 contained a 16-bp insertion sequence shown in blue. Clones #14 and #21 conferred 43-bp and 19-bp deletions, respectively, shown in red. (C) DNA sequences of the bi-allelic deletion clone. This clone was obtained from the clone #14 with an additional 1-bp deletion in the counterpart allele, as indicated by an arrow. (D) DNA sequences before editing, of mono-allelic deletion (#14 clone) and bi-allelic deletion (KO). While arrows, the position of the first deletion. Black arrow, the position of the single nucleotide deletion in the 2nd edit. (E) RT-qPCR analysis of *Mmp3* mRNA in the parental LuM1 cells and the MMP3-KO cells. The mRNA level of Mmp3 was decreased, while the mutant mRNA of *Mmp3* was detectable. The relative mRNA levels were normalized to *Gapdh* as an internal control. *p<0.05, n=6. (F) Western blot showing MMP3 in the cell lysates. Arrowhead indicates full-length MMP3 (54 kDa). The experiments were repeated thrice in Fig. 3E, F.

Preprints (www.preprints.org) | NOT PEER-REVIEWED | Posted: 19 February 2020 doi:10.20944/preprints202002.0281.v1

Peer-reviewed version available at Cancers 2020, 12, 881; doi:10.3390/cancers12040881

2.4. MMP3 positively regulates the expression and secretion of CCN2/CTGF from the metastatic colon cancer cells.

It has been shown that MMP3 positively regulates *CCN2/CTGF* gene expression in chondrocytes [26]. We therefore next examined whether gene expression of cellular communication network (CCN) gene family members composed of CCN1 to CCN6 could be altered between Colon26 and LuM1 or by the targeted deletion of MMP3. Among the six CCN family members, the transcript levels of *Ccn2/Ctgf* and *Ccn5/Wisp2* were higher in LuM1 cells than those in Colon26 cells (Fig. 4 A, B). In contrast, the transcript levels of *Ccn1/Cyr61, Ccn3/Nov,* and *Ccn4/Wisp1* were diminished in LuM1 cells.

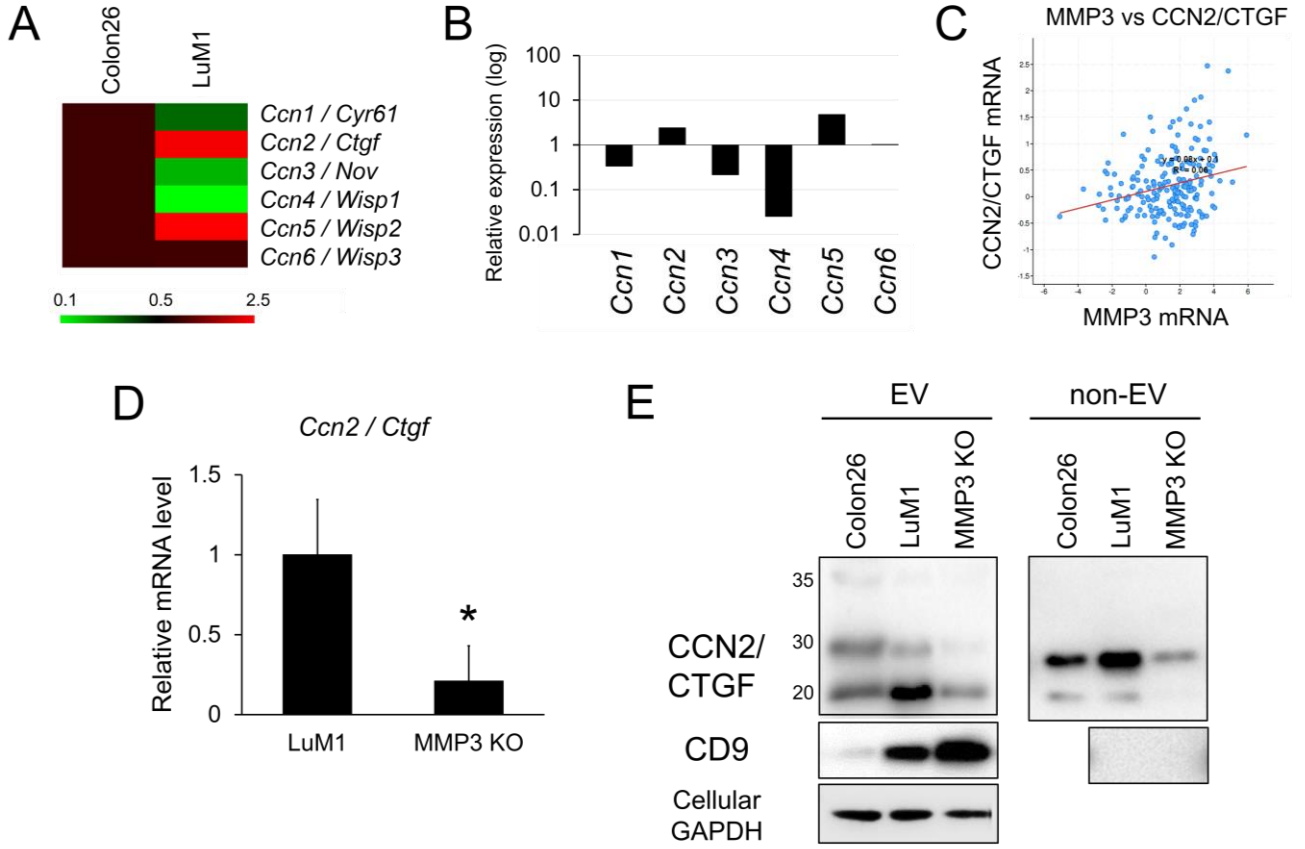

Fig. 4 | MMP3 knockout diminished gene expression and secretion of CCN2/CTGF. (A to C) Positively correlation between MMP3 and CCN2/CTGF expression. (A) Heat map analysis of the cell communication network (CCN) gene family members between LuM1 vs. Colon26 cells. The data were from microarray analysis. (B) Relative mRNA expression levels of CCN gene family members in LuM1 vs. Colon26 cells. (C) Scatter plot analysis showing co-expression correlation between MMP3 vs. CCN2/CTGF in patients-derived tumor samples of colorectal adenocarcinomas (632 cases). (D) RT-qPCR analysis of *Ccn2/Ctgf* transcripts expressed in LuM1 vs. MMP3 KO cells. n=6, *p<0.05. (E) Western blot analysis of CCN2/CTGF and CD9 in EV and non-EV fractions. Production of the C-terminal TSP1-CT fragments (20 to 25 kD) of CCN2 was altered between Colon26 and LuM1 cells or MMP3-KO. The experiments were repeated twice in Fig. 4D, E.

We next examined the co-expression correlation between *MMP3* and *CCN2/CTGF* among 632 tumor samples derived from 632 colorectal adenocarcinoma patients registered in the cancer genome atlas (TCGA). There was co-expression correlation significance between *MMP3* and *CCN2/CTGF* (Fig. 4C, $y = 0.08x + 0.1$) in the colorectal adenocarcinoma cases, suggesting that MMP3 may positively regulate CCN2/CTGF expression both in human colorectal adenocarcinoma cases and in the mouse colorectal adenocarcinoma model. Consistently, the transcript level of *CCN2/CTGF* was significantly lowered in the MMP3-KO cells as compared to LuM1 cells (Fig. 4D).

It has been shown that MMPs are able to cleave CCN2/CTGF in the middle of the protein, separating N-terminal IGFBP-VWC modules and C-terminal TSP1-CT modules [28]. We detected the C-terminal half fragments (approx. 20 to 25 kD, including the TSP1-CT modules) of CCN2/CTGF in EV and non-EV fractions of LuM1 cells at higher levels as compared to those derived from Colon26 or MMP3-KO cells (Fig. 4E, Fig. S4). These data suggested that MMP3 exerted at least two functions, including the up-regulation of CCN2/CTGF at the transcriptional level and also the processing of the same factor at the post-translational level. However, the level of CD9 was higher in the MMP3-KO cells-derived EVs as compared to LuM1-EVs. Total protein concentration in the EV fraction was not altered by MMP3 KO (Fig. S5).

These data indicated that MMP3 positively regulates CCN2/CTGF transcription and the release of the C-terminal TSP1-CT fragment of CCN2/CTGF from the metastatic colon cancer cells, suggesting intracellular moonlighting roles for MMP3 at both transcriptional and post-translational levels.

2.5. The anti-tumor effect of MMP3-Knockout in vitro and in vivo.

To elucidate the potential role of MMP3-KO in tumor progression, we examined whether the knockout of MMP3 could alter the proliferation, migration, invasion in vitro, and tumor growth in vivo. MMP3-KO cells grew more slowly to Day 5 as compared to LuM1 cells (Fig. 5A). In addition, the knockout of MMP3 significantly inhibited tumor growth in mice in the allograft model (Fig. 5B). Cellular migration and invasion were also significantly inhibited by the deletion of MMP3 as compared to the MMP3-high LuM1 cells (Fig. 5 C, D).

These data evidently indicate that MMP3 plays a key role in tumor progression including migration, invasion, and tumor growth, while MMP3-KO is an effective anti-tumor method targeting aggressive adenocarcinoma.

Preprints (www.preprints.org) | NOT PEER-REVIEWED | Posted: 19 February 2020 doi:10.20944/preprints202002.0281.v1

Peer-reviewed version available at Cancers 2020, 12, 881; doi:10.3390/cancers12040881

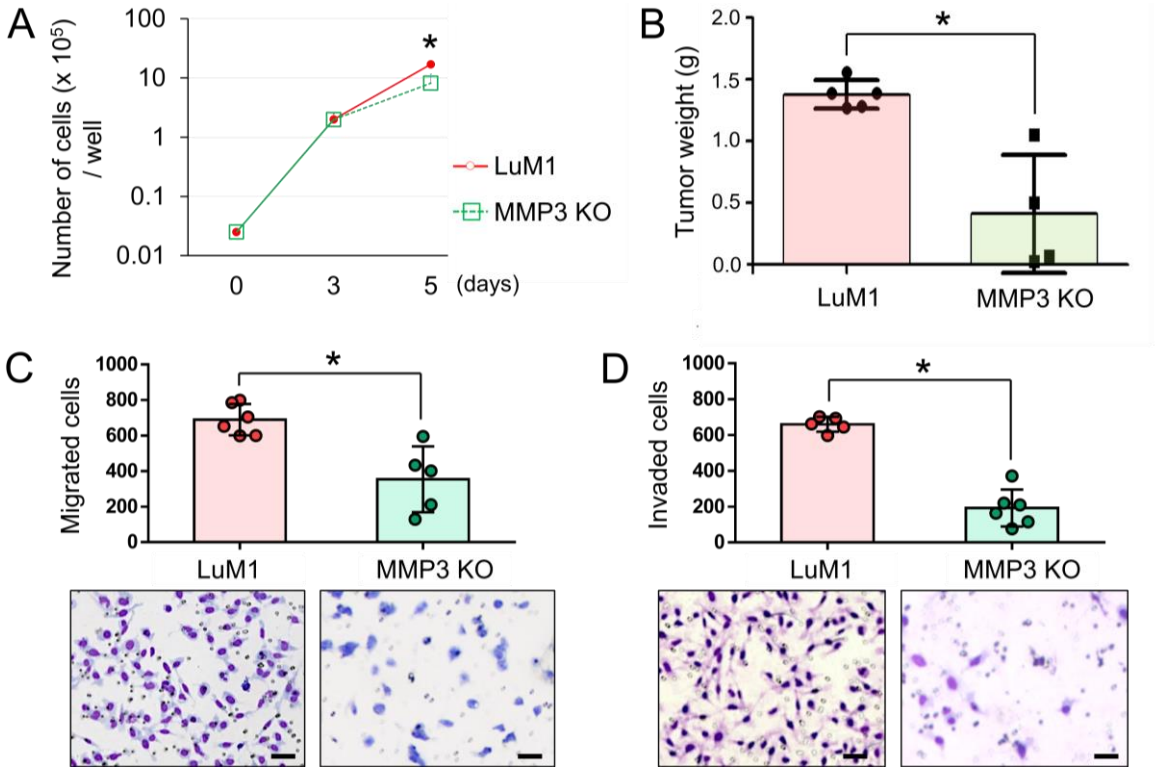

Figure 5 | The knockout of MMP3 suppressed tumor progression. (A) Growth curves of LuM1 cells and MMP3 KO cells. n=3. *p<0.05. (B) Subcutaneous tumor weights of LuM1 vs. MMP3-KO cells in the allograft model. Tumor weights were measured on day 21 after the injection. LuM1 group, n=6; MMP3 KO group, n=5. *p<0.05. (C) Column scatter plot of *in vitro* migration activities altered by MMP3 knockout. Top, the number of migrated cells. n=5, *p<0.05. Bottom, representative images of migrated cells stained with Diff-Quick. Scale bars, 50 μm. (D) Column scatter plot of *in vitro* invasion activities. Top, the number of invaded cells. n=5, *p<0.05. Bottom, representative images of invaded cells stained with Diff-Quick. Scale bars, 50 μm. The experiments were repeated twice in Fig. 5A, B and thrice in Fig. 5C, D.

2.6. Oncosome-mediated intranuclear transfer of MMP3

It has been shown that MMP3 possesses six NLS and that extracellular MMP3 could translocate into cellular nuclei, where MMP3 positively regulated *CCN2/CTGF* gene [26]. However, it was uncertain whether oncosomes were involve in the intranuclear transfer of MMP3. We therefore next examined whether MMP3 enriched in LuM1-derived oncosomes could be transferred into MMP3-null recipient cells and intranuclearly. We conformed that MMP3 was undetectable in the cell lysate, EVs and non-EV fractions of MMP3-KO cells while being markedly detectable in those of LuM1 cells (Fig. 6A; Fig. S6, S7).

Both LuM1 and MMP3-KO cells released EVs with cup-shaped morphology sized between 50 to 300 nm observed under TEM (Fig. 6B). However, particle diameter distribution analysis revealed that the size of LuM1-EVs was peaked at 146.6 nm while that of MMP3-KO-EVs was enlarged to 164.2-nm diameter (Fig. 6C), suggesting that deletion of MMP3 might result in retention of proteins on or in the vesicles.

Preprints (www.preprints.org) | NOT PEER-REVIEWED | Posted: 19 February 2020 doi:10.20944/preprints202002.0281.v1

Peer-reviewed version available at Cancers 2020, 12, 881; doi:10.3390/cancers12040881

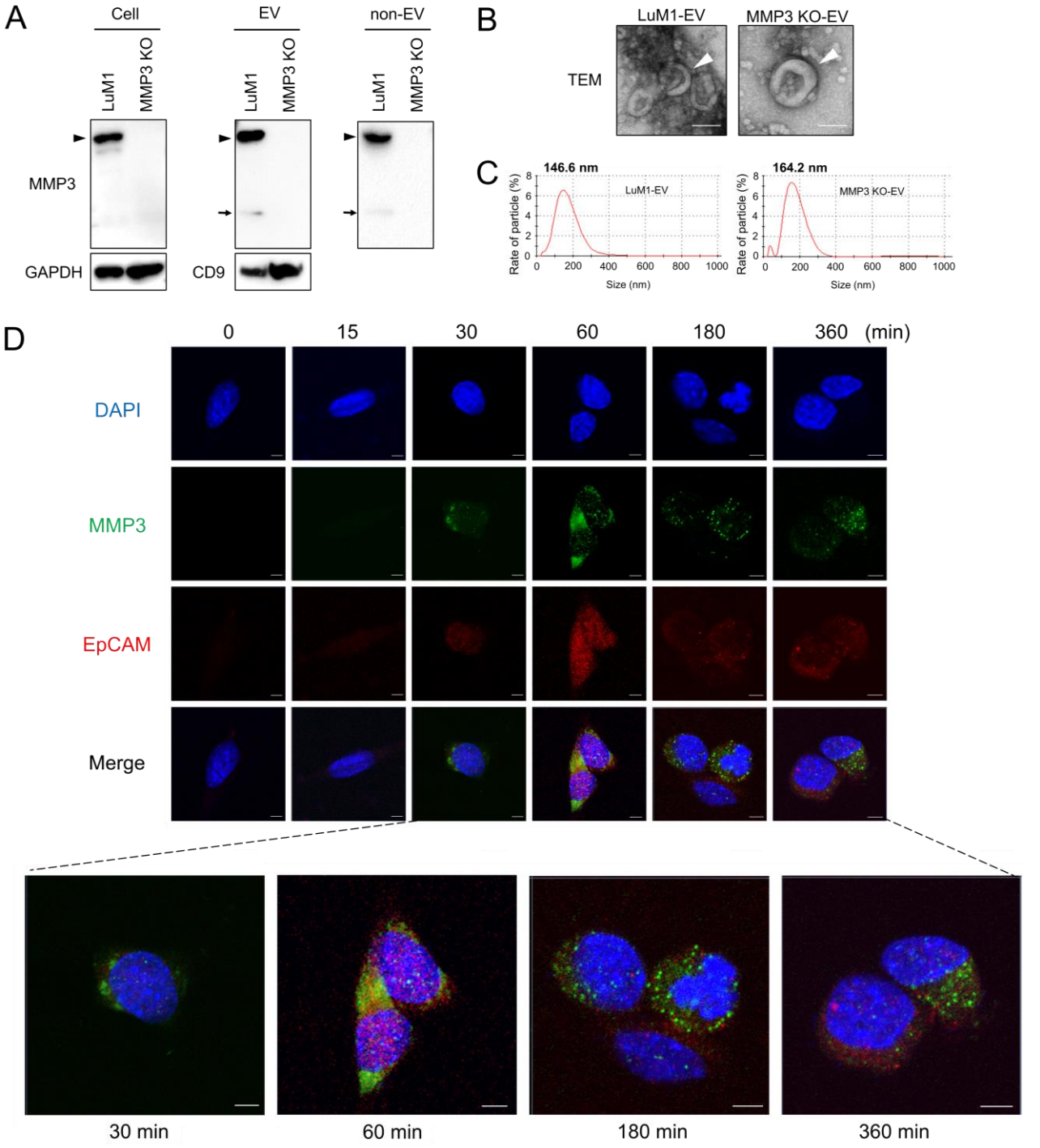

Figure 6 | Oncosomal delivery of MMP3 to the recipient cells intranuclearly. (A) Western blotting of MMP3 and CD9 in cell lysate, EVs and non-EV fractions. Arrowheads indicate full-length MMP3 (54 kDa). Arrows indicate the C-terminal PEX fragment of MMP3. (B) Representative TEM images of EV fractions derived from LuM1 and MMP3-KO cells. Arrowheads indicate vesicles with cup-shaped morphology. Scale bars, 100 nm. (C) Particle diameter distribution analysis of EV fractions. (D) Oncosome-mediated intranuclear transfer of MMP3. LuM1-derived MMP3-rich oncosomes were added into culture media of MMP3-KO recipient cells at a final concentration of 20 μg/mL. Cells were fixed at each time point. Immunocytochemistry of MMP3 (green) and CD326/EpCAM (red) was carried out. Blue, DAPI. The images were taken under confocal laser scanning microscopy. Scale bars, 5 μm. The experiments were repeated twice in Fig. 6A, D.

Preprints (www.preprints.org) | NOT PEER-REVIEWED | Posted: 19 February 2020 doi:10.20944/preprints202002.0281.v1

Peer-reviewed version available at Cancers 2020, 12, 881; doi:10.3390/cancers12040881

We next investigated whether MMP3 in/on LuM1-oncosomes could be molecularly transferred into MMP3-null recipient cells and into nuclei. MMP3 was detected mainly in the cytoplasm but also in nuclei of the recipient cells at 30 minutes to 6 hours after the addition of LuM1-oncosomes (Fig. 6D, green), suggesting that oncosomal MMP3 could be first taken into endosomes and then some endosomally located molecules could escape to nuclei.

It has been shown that a single-pass transmembrane glycoprotein CD326/EpCAM was often enriched in oncosomes derived from cancer stem cells [CSC, also known as cancer-initiating cells (CIC)] and a cleaved intracellular domain of CD326/EpCAM was able to translocate intranuclearly to then exert transcriptional control [35,36]. We therefore next examined the subcellular distribution of CD326/EpCAM upon the addition of the LuM1-oncosomes. CD326/EpCAM was barely detectable in the MMP3-null cells at 0 min while being increased at 30 min to 6 hours after the addition of LuM1-oncosomes (Fig. 6D, red). The co-localization of CD326/EpCAM and MMP3 was detected in the cytoplasm (supposed to be endosomes), but not in nuclei (Fig. 6D, arrowheads).

These data indicate that the pro-tumorigenic moonlighting metalloproteinase was deliverable from oncosomes to recipient cells intranuclearly.

2.7. Oncosome-mediated transfer of MMP3 induces expression of CCN2/CTGF.

In order to demonstrate oncosomal MMP3-driven induction of CCN2/CTGF, we next examined whether the levels of MMP3 and CCN2/CTGF were altered by the transmission of LuM1-oncosomes into MMP3-null recipient cells. MMP3 was becoming stably detectable in the recipient cells at 15 min to 9 hours after the addition of oncosomes (Fig. 7 A, B). The protein level of CCN2/CTGF (approx. 38 kD, potentially de novo synthesized full-length CCN2/CTGF) was also increased in the recipient cells at 15 min to 1 hour after the addition of LuM1-oncosomes, although thereafter decreaseing at 3 to 9 hours (Fig. 7 A, B; Fig. S8). The anti-CCN2/CTGF antibody detected the approx. 38-kD, potentially de novo synthesized full-length CCN2/CTGF in the recipient cells, although the LuM1-oncosomes did not contain the full-length CCN2/CTGF. Consistently, CCN2/CTGF was under the detection limit in the EVs in LC-MS/MS analysis (Table 2).

Table 2 | Protein MS/MS scores of EV fractions derived from LuM1 vs MMP3-KO cells.

Protein name	LuM1-derived EVs	MMP3-KO cell-derived EVs
MMP3 / stromelysin 1 (STR1)	23.66	N.D.
CCN2 / CTGF / FISP12	N.D.	N.D.
ACTBL2	20.21	19.79

N.D. not detected.

Preprints (www.preprints.org) | NOT PEER-REVIEWED | Posted: 19 February 2020 doi:10.20944/preprints202002.0281.v1

Peer-reviewed version available at Cancers 2020, 12, 881; doi:10.3390/cancers12040881

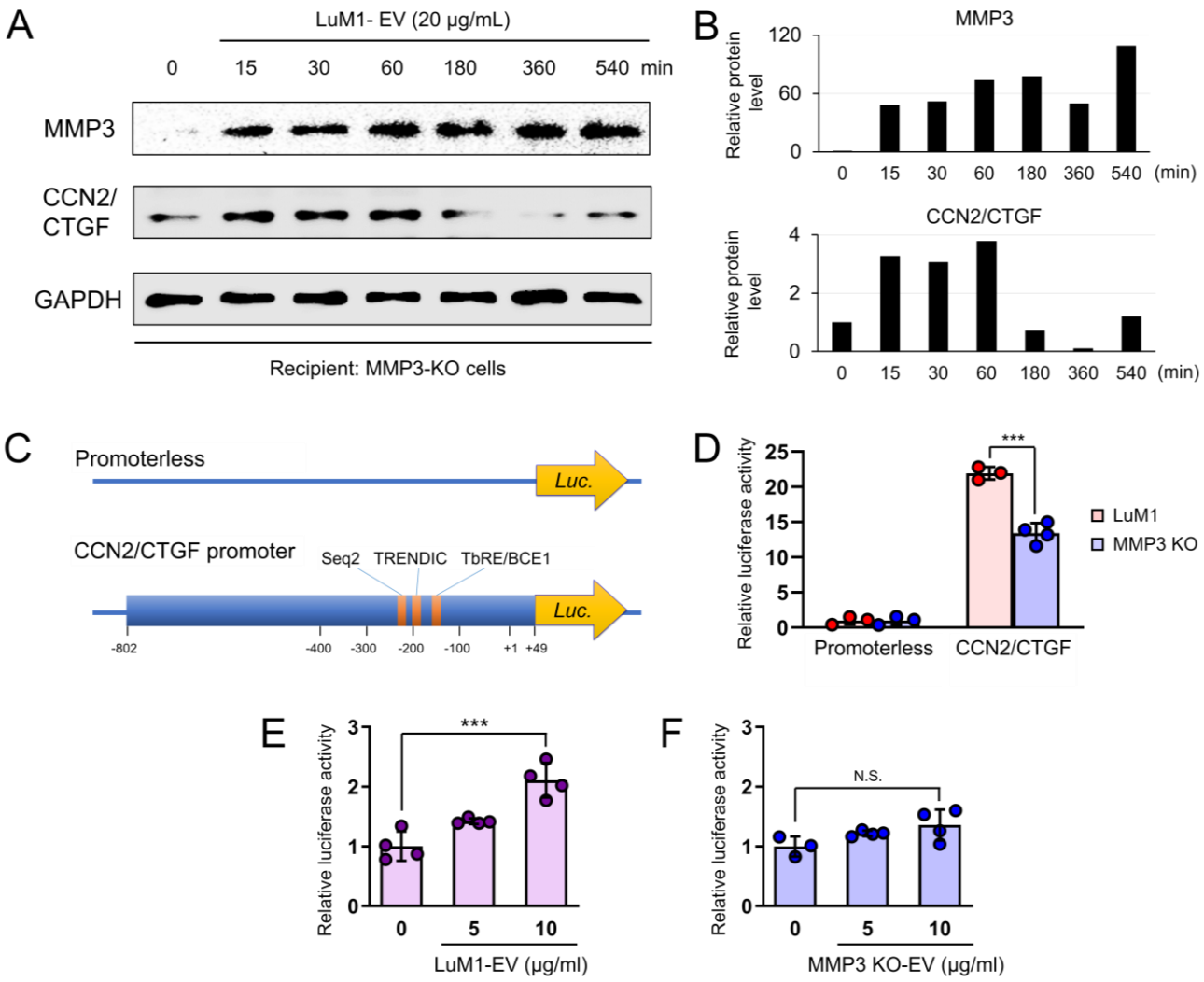

Figure 7 | Oncosomal delivery of MMP3 induced the expression of CCN2/CTGF through transcriptional activation. (A) Western blotting showing MMP3 and CCN2 in the recipient cell lysate. LuM1-derived MMP3-rich oncosomes were added to culture media of the MMP3-null recipient cells at a final concentration of 20 μg/mL. Cells were lysed at each time point (0, 15, 30, 60, 180, 540 min) after the addition of oncosomes. The basal level of full-length CCN2 (38 kD) was very low while being induced upon the addition of oncosomes. (B) The band intensities of MMP3 and CCN2. Band intensities of panel A were measured by using ImageJ. The values relative to GAPDH were shown. (C) Schemes of reporter constructs. Top, a promoterless construct, pGL3-basic. Bottom, CCN2/CTGF promoter-driven luciferase (Luc) reporter construct. Seq2, TRENDIC, and TbRE/BCE1 are cis-elements potentially bound by MMP3. (D) Relative luciferase activities from CCN2/CTGF promoter-Luc or promoterless constructs. LuM1 cells were transfected with the reporter constructs and phRL-TK. Values are expressed as Mean±SD, relative to promoterless. ***P<0.001, n=3 to 4. (E, F) Effects of LuM1-EV and MMP3-KO-EV on the CCN2/CTGF promoter activity. The MMP3 KO cells were transfected with the CCN2/CTGF promoter-Luc construct. LuM1-derived EV (E) or MMP3 KO cells-derived EV (F) at the final concentrations of 0, 5 or 10 μg/ml were added to the sefum-free culture media. Values are expressed as Mean±SD, relative to EV 0. ***P<0.0001, n= 3 to 4. The experiments were repeated twice in Fig 7A, D, E.

Preprints (www.preprints.org) | NOT PEER-REVIEWED | Posted: 19 February 2020 doi:10.20944/preprints202002.0281.v1

Peer-reviewed version available at Cancers 2020, 12, 881; doi:10.3390/cancers12040881

311 To investigate the MMP3-CCN2 regulatory axis, we next examined whether the activity of CCN2/CTGF
312 promoter, containing MMP3-binding sequences, was altered by the deletion of MMP3 gene or by delivery of r
313 MMP3-rich EVs. The CCN2/CTGF promoter-driven luciferase reporter activity was significantly lower in
314 MMP3-KO cells than that in the parental LuM1 cells (Fig. 7 C, D). MMP3-rich, LuM1-derived EVs (at a final
315 concentration of 10 μg/ml) significantly increased the activities of the CCN2/CTGF promoter (Fig. 7E), while
316 MMP3-null EVs did not.
317 These data thus indicate that MMP3 is deliverable from oncosomes into the nuclei of recipient cells,
318 activates the CCN2/CTGF transcription, and then up-regulates the expression of CCN2/CTGF.

319 **2.8. Clinical significance of MMP3 expression**

320 To investigate the clinical significance of MMP3 expression, we next searched TCGA databases of MMP3
321 expression in patient-derived tumor samples. Tumor MMP3 mRNA expression levels were at relatively high
322 levels in head and neck cancer (HNC), stomach cancer, cervical cancer, pancreatic cancer, colorectal cancer,
323 lung cancer, urothelial cancer, breast cancer, endometrial cancer, melanoma, glioma, prostate cancer, as
324 compared to ovarian cancer or testis cancer (Fig. 8A).
325 We next carried out survival analyses using the Kaplan-Meier plot. High expression of MMP3 was
326 prognostic, unfavorable in pancreatic cancer (P=0.00041) and cervical cancer (P=0.00097) (Fig. 8 B, C; Table
327 3). The 5-year survival of MMP3-low pancreatic cancer patients was 34%, while that of MMP3-high group was
328 11%. The 5-year survival of MMP3-low cervical cancer patients was 71%, while that of MMP3-high group was
329 51%. We could not find expression-survival correlation in other types of cancers, although this was conceivable
330 due to sub-types and stages (i.e. non-metastatic or metastatic) of cancers.
331

332 **Table 3** | MMP3 expression correlated with poor prognosis

	Pancreatic cancer	Cervical cancer
P value	0.00041	0.00097
5-year survival (MMP3 low)	34%	71%
5-year survival (MMP3 high)	11%	51%

333

334

Preprints (www.preprints.org) | NOT PEER-REVIEWED | Posted: 19 February 2020 doi:10.20944/preprints202002.0281.v1

Peer-reviewed version available at Cancers 2020, 12, 881; doi:10.3390/cancers12040881

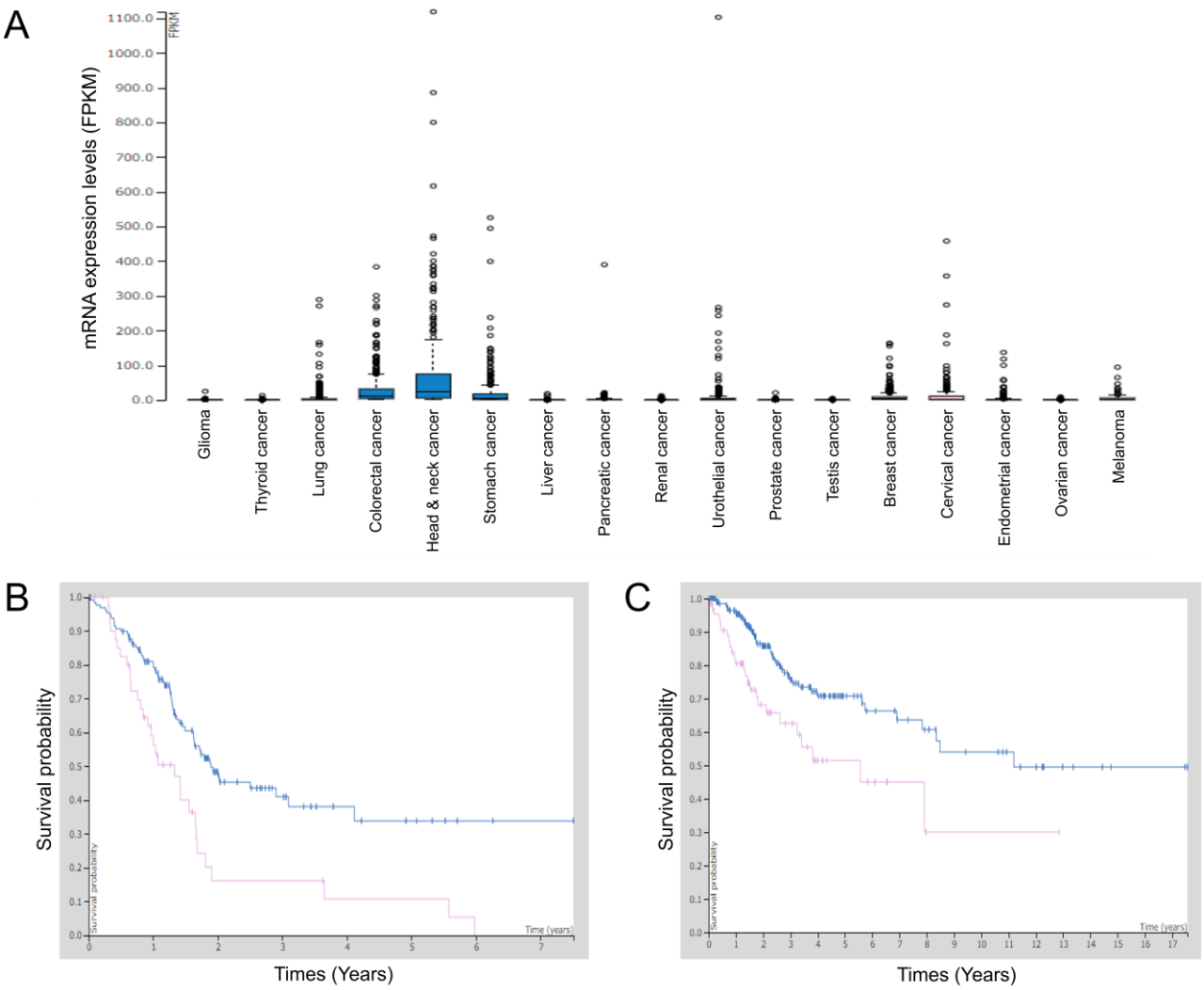

335 **Figure 8 | Clinical significance of MMP3 expression** (A) MMP3 mRNA expression levels in patient-derived tumor
336 specimens. Values indicate Fragments per kilo base per million mapped reads (FPKM) of RNA-seq. (B, C) Kaplan-Meier
337 survival curves of patients suffering from pancreatic cancer (B) and cervical cancer (C). Data were obtained from TCGA and
338 Human Protein Atlas databases.

339 ## 3. DISCUSSION

340 Our study indicates for the first time that aggressively malignant cancer cells can release oncosomes enriched
341 in MMP3 that potentially penetrate the tumor microenvironment, cross biological barriers, and become enriched
342 in distant organs. Oncosomal MMP3 also plays transcriptional roles in the induction of the cell communication
343 network factor CCN2/CTGF, a finding which may be important for understanding a mechanism of tumor-
344 stroma progression and metastasis. Our study indicates that the rapidly metastatic cells-derived, MMP3-rich
345 oncosomes were rapidly transmissive, invasive to tissues and cells, and powerfully pro-tumorigenic, suggesting
346 that MMP-rich oncosomes involve primary and secondary tumorigenesis. In our current data, LuM1-oncosomes

Peer-reviewed version available at Cancers 2020, 12, 881; doi:10.3390/cancers12040881

significantly promoted tumor growth through body fluids and caused cachexia in the mice, accompanied by systemic distribution of the oncosomes into multiple organs, including liver, lung, and head. Indeed, LuM1-oncosomes delivering MMP3 altered the character of the recipient cells, represented by the immediate induction of an additional pro-tumorigenic factor, CCN2/CTGF. Interestingly, the transferred MMP3 was sustained from 15 min to 9 hours post-oncosome-addition period, whereas the induction of CCN2/CTGF was transient from 15 min to 1 hour, suggesting that CCN2/CTGF might be secreted from the cells upon the synthesis or switched off by regulatory mechanisms. The current data showing intranuclear delivery of MMP3 were confirmed under CLSM and are consistent with our previous study that MMP3 possesses functional NLSs and is able to translocate into cellular nuclei, where the relocated MMP3 positively regulates *CCN2/CTGF* and *HSP* gene [26,27,37]. Our current data indicate that oncosomes are able to deliver MMP3 from aggressive cancer cells to recipient cells, where MMP3 induces expression of CCN2/CTGF, consistent with a previous study demonstrating MMP3 responsive element in the promoter region of CCN2/CTGF gene [30-32].

Our data suggested that tumor-derived oncosomes have the potential to reprogram recipient cells. MMPs were previously identified in EVs released from various cell types, some of which possessed proteolytic activities [38,39]. EVs derived from 8701-BC breast cancer cells and HT-1080 fibrosarcoma cells were reported to contain MMP9 in both pro- and mature forms with proteolytic activity [39,40]. However, MMP3 has been identified in/on EVs released from stromal cells such as mesenchymal stem cells (MSC) and adipocytes[41,42]. Moreover, cancer exosomes triggered MSC differentiation into pro-angiogenic and pro-invasive myofibroblasts secreting high levels of matrix regulating factors (MMP-1, -3 and -13), VEGF-A, and HGF [43]. A recent study reported MMP3 to be up-regulated in both stromal fibroblasts and cancer cells by oxidative stress [44]. Moreover, CCN2/CTGF can be produced from both tumor and stromal cells. MSC-derived CCN2/CTGF promoted tongue squamous cell carcinoma progression [45]. Another study reported that tumor-derived CCN2/CTGF could mediate tumor-stromal interactions which accelerate hepatocellular carcinoma progression [46]. Notably, it has been recently postulated that CCN2/CTGF might contribute to colorectal cancer progression, especially in a fibrotic consensus molecular subtype [47]. Thus, MMP3, CCN2/CTGF, and their oncosomes can be produced on both sides of the interaction to promote tumor-stroma malignant conversion. It is conceivable that the knockout of MMP3 can efficiently interrupt the pro-malignant communication between tumor and stroma.

We also observed that the levels of CD326/EpCAM, a marker of cancer stem cells and tumor-derived exosomes, increased in the cells and nuclei upon oncosomal transfer, although it is uncertain whether CD326/EpCAM was transferred from oncosomes or de novo synthesized in the recipient cells. Nevertheless, CD326/EpCAM was detected in the cytoplasm and nuclei at 30 min to 6 hours post-oncosome-addition period, suggesting that MMP3 and CD326/EpCAM were co-transferred from the oncosomes to the recipient cells. It

has been shown that CD326/EpCAM is a single-pass transmembrane glycoprotein, often enriched in oncosomes derived from CSC/CIC, while CD326/EpCAM intracellular domain is able to translocate to the nucleus forming transcriptional complex with β-catenin, a process which activates the stemness genes [35,36]. Thus, the LuM1-derived oncosomes could contain MMP3 and CD326/EpCAM, whose transfer may induce stemness in the recipient cells in the local tumor microenvironment and in distant organs. There are two potential mechanisms of MMP3 transmission, including: (i) MMP3 contains six NLS, basic amino acid clusters [26,27], which could work as membrane-permeable, membrane disrupting translocase/flippase as in the Trans-Activator of Transcription Protein (TAT) peptide, also called Cell Penetrating Peptide (CPP) [48], and/or (ii) proteolysis by MMP3 might contribute to endosomal escape as with other proteinases; cathepsins, are essential for the endosomal escape of virus [49,50].

Our data also touch upon key proteolytic activities of the metalloproteinase in the oncosomes. The PEX fragment of MMP3 was found in/on the oncosomes in significant amounts. It has been shown that metalloproteinases including MMP3 possess a self-cleavage, self-activation mechanism [21,26]. Therefore, it is conceivable that the PEX fragment in the oncosomes is a functional remnant (metabolite) indicating on-oncosome proteolysis by metalloproteinases. The C-terminal half fragments of CCN2 in/on oncosomes and non-vesicular extracellular fractions are also potentially functional remnants generated by the metalloproteinase activity. Consistently, it has been shown that active MMPs cleave CTGF to generate a N-terminal half fragment containing IGFBP-VWC modules and another C-terminal fragment composed of TSP1-CT modules, a bioactive fragment essential for angiogenesis [25,28,51,52]. It has been also shown that the C-terminal half fragment of CTGF promoted osteoclastogenesis [29]. Thus, the oncosome-associated CTGF fragments, found in our study, may play a key role in tumor-stroma interaction. However, our study has not determined a key binding partner for CCN2/CTGF which is able to bind with a number of partners including CCN homo-/hetero-dimerization, integrins, EGFR, Notch, LRP1/6, fibronectin, BMP2/4, TGFβ, FGF2, or aggrecan [53]. In contrast, MMPs cleave a number of extracellular proteins including extracellular matrix (ECM: collagen, proteoglycan, etc.), matricellular proteins (osteopontin [54], CCN2/CTGF [28]), transmembrane proteins (E-cadherin, pro-HB-EGF), growth factors (latent TGFβ), and an immune checkpoint protein (PD-L1) [55]. Thus, CCN2 and MMP3 may regulate matricellular balance in the vesicular microenvironment. Our data also indicate that deletion of MMP3 increased the size of EVs and the volume of EV proteins (Fig. S1), suggesting that proteolytically active MMPs cleave out proteins on/in the vesicles at extracellular space, while deletion of MMP3 resulted in the retention of proteins on/in the vesicles. Indeed, CD9 was increased in the MMP3-null EVs. Therefore, it is conceivable that LuM1-EVs contained substrate proteins cleavable by MMP3 on/in the vesicles. Thus, the presence or absence of MMPs in/on the vesicles markedly alters the properties of the EVs at proteome and functional levels.

In conclusion, oncosomes enriched with moonlighting metalloproteinase MMP3 are transmissive, pro-tumorigenic, and inducing cellular communication network factor 2, which is essential for tumor-stromal interaction and progression.

4. MATERIALS AND METHODS

4.1. Cells

A murine colon cancer cell line Colon26 (also known as CT26) and a rapidly metastatic subline LuM1 were maintained in RPMI1640 with 10% FBS supplemented with penicillin, streptomycin, and amphotericin B [34,56,57]. MMP3-knockout LuM1 (MMP3 KO) cells were generated using the genome-editing method as described below and maintained in RPMI1640 with 10% FBS supplemented with penicillin, streptomycin, and amphotericin B.

4.2. Genome editing

DNA oligonucleotides used for guide RNA (gRNA) synthesis were designed with the GeneArt™ clustered regularly interspaced short palindromic repeat (CRISPR) gRNA Design Tool (Table 4).

Table 4. The sequence of gRNA

Name of primers	5’ to 3’ sequences
gRNA #1	TCCCTTGCACTGTCATGCAA
gRNA #2	CAAGGCCATAGTAGTTTTCT

The gRNAs were then synthesized using the GeneArt™ precision gRNA synthesis kit (ThermoFisher). CRISPR RNA (crRNA) / trans-activating crRNA (tracrRNA) hybridization and ribonucleoprotein (RNP) complex formation was done according to the manufacturer’s instructions. For transfection, 8×10^4 cells were seeded in 24-well plates and incubated overnight. Cells were then transfected with the RNP composed of gRNA (125 ng) and recombinant Cas9 nuclease (rCas9; 500 ng) using the CRISPRmax transfection reagent (ThermoFisher). The genomic cleavage efficiency was measured by a PCR-based method using the GeneArt® Genomic Cleavage Detection (GCD) kit (ThermoFisher) according to the manufacturer's instructions. Cells were corrected at 48 h post-transfection and PCR was carried out. The amplicon was loaded to 2% agarose gel electrophoresis. The cleavage efficiencies were calculated based on the relative band intensities, quantified using Image J. Isolation of the single clone was carried out by dilution cloning method using 96 well plate. Genomic DNA was extracted from each clone by using a DNeasy Blood & Tissue Kit (Qiagen). Exon 1 of *Mmp3* in each clone were amplified using Blend Taq Plus (Toyobo, Osaka, Japan) and GCD primer sets under the following conditions in the

Peer-reviewed version available at Cancers 2020, 12, 881; doi:10.3390/cancers12040881

thermal cycler: an initial denature at 95°C for 10 min, 30 cycles (at 95°C for 30 sec, at 55°C for 30 sec, and at 72°C for 30 sec), followed by final extension at 72°C for 7 min. PCR products were cleaned up using ExoSAP-ITTM Express PCR Product Cleanup Kit (ThermoFisher). The sequences of each clone were analyzed by Sanger sequencing method. To establish a bi-allelic deletion, gRNA/rCas9 and pEGFP-c1 vector were cotransfected into a heterogenic deletion clone (-43; clone #14) in three different conditions shown in Fig. S1c by using NEPA21 electroporator (NEPA Gene, Ichikawa, Japan). Cells were cultured and selected within G418 antibiotics at a concentration of 0.5 mg/ml for 20 days. DNA extraction, PCR, and sequencing were performed as described above.

4.3. Isolation of EV

EV fraction was prepared using a modified polymer-based precipitation method as described [13]. Briefly, cells growing in two 10-cm dishes were washed with PBS (-), and then further cultured in 4 mL of serum-free medium per dish for 2 days. Cell culture supernatant was centrifuged at 2,000 × *g* for 30 min at 4°C to remove detached cells. The supernatant was then centrifuged at 10,000 × *g* for 30 min at 4°C to remove cell debris. In the PBP method, the supernatant (8 mL) was concentrated to less than 1 mL by using an Amicon Ultra-15 Centrifugal Filter Devices for M.W. 100k (Merk Millipore, Burlington, MA). The concentrate was applied to Total EV fraction Isolation (ThermoFisher, Waltham, MA). The pass-through was concentrated using an ultrafiltration device for molecular weight 10 kD and used as a non-EV fraction. The EV fraction was suspended in 100 µL PBS (-). Protein concentration was measured using microBCA protein assay kit (ThermoFisher).

4.4. Transmission electron microscopy

As described previously [14], a 400-mesh copper grid coated with formvar/carbon films was hydrophilically treated. The EV suspension (5-10 µL) was placed on Parafilm, and the grid was floated on the EV liquid and left for 15 min. The sample was negatively stained with 2% uranyl acetate solution for 2 min. EV fraction on the grid was visualized with 20,000 times magnification with an H-7650 transmission electron microscope (TEM) (Hitachi, Tokyo, Japan) at the Central Research Laboratory, Okayama University Medical School.

4.5. Particle diameter distribution

As described previously [4], forty microliters of EV fraction within PBS (-) was used. Particle diameters of the EV fractions in a range between 0 and 1,000 nano-diameters were analyzed in Zetasizer nano ZSP (Malvern Panalytical, UK).

4.6. Immunocytochemistry and confocal laser scanning microscopy

Cells were seeded at concentrations of 4.0×10^4 per well in a 24-well-plate and then incubated overnight. LuM1-derived EV fraction was added to culture media in a 24-well plate at a concentration of 20 μg/mL and then cells were cultured for 0, 15, 30, 60, 180, 360, and 540 min. Cells were then fixed with 4% paraformaldehyde in PBS for 10 min at each time point after the addition of EVs. Immunocytochemistry and CLSM were carried out as described [21,26]. Briefly, cells were permeabilized with 0.5% Tween-20 in PBS for 5 min. The fixed cells were blocked in 10% normal goat serum solution for 30 min and then incubated overnight at 4°C with rabbit anti-MMP3 antibody (EP1186Y, ab52915, Abcam) and mouse anti-CD326/EpCAM antibody (EGP40/1110, Abgent) in 10% normal goat serum solution. Cells were then incubated with anti-rabbit IgG AlexaFluor488 [Cell Signaling Technology (CST), Danvers, MA] or anti-mouse IgG AlexaFluor594 (CST) for 1 hour at room temperature. Cellular Nuclei were stained with 4', 6-diamidino-2-phenylindole (DAPI; Invitrogen, Carlsbad, CA). The fluorescence was analyzed using a CLSM imaging system LSM 780 META (Carl Zeiss, AG, Jena, Germany). To define MMP3 or CD326/EpCAM positivity, the fluorescence intensity of the cells without the primary antibodies were subtracted as background.

4.7. EV-mediated molecular transfer. EV-mediated molecular transfer was performed as previously described [6]. Colon26 cells were seeded at a concentration of 4.0×10^4 cells per well in a 24-well plate and incubated overnight. LuM1-derived EV fraction (8 or 20 μg/mL) was added to the culture media. Cells were cultured for 9 h and the medium was replaced with serum-free medium. Cells were cultured for 2 days and then lysed in RIPA buffer for western blotting.

MMP3 KO cells were seeded at a concentration of 1.2×10^6 cells per dish in a 10 cm dish and incubated overnight. LuM1-derived EV fraction was added to the culture media at a final concentration of 20 μg/mL. The recipient cells were lysed with RIPA buffer at 0, 15, 30, 60, 180, 360, and 540 min post-EV-addition period for western blotting.

4.8. Luciferase reporter assay

Luciferase assay was carried out as previously described [26,30,32,58]. Briefly, LuM1 or MMP3 KO cells were seeded at 2×10^4 cells per well in a 96-well plate and cultured for 24 h in RPMI 1640 medium with 10% FBS. The CCN2/CTGF promoter-driven luciferase expression reporter construct (pTS589, 100 ng/well) [26,30-32] or the promoterless vector PGV-B2 (Nippon Gene, Tokyo, Japan; 100 ng/well) were cotransfected with an internal control vector phRL-TK (Promega, Madison, WI; 20 ng/well) using Lipofectamine 3000 transfection reagent (ThermoFisher). Media were replaced with RPMI 1640 without FBS and EVs were added to the media at concentrations of 0, 5 or 10 μg/mL and cells were incubated for 24 h. Cells were lysed and luciferase activities were measured using Dual-Luciferase Reporter Assay System (Promega, Madison, WI).

Peer-reviewed version available at Cancers 2020, 12, 881; doi:10.3390/cancers12040881

4.9. EV labeling

EV labeling and transmission experiments were carried out as described previously [4,33]. For in vitro imaging, 20 μg of EV fraction was incubated with 10 μM BODIPY TR Ceramide (ThermoFisher) for 20 min at 37°C. For in vivo imaging, 15 μg of EV fraction was incubated with 5 μM Cy7 Mono NHS Ester (GE Healthcare) for 90 min at 37°C. The unincorporated dye was removed using Exosome Spin Columns (MW. 3,000) (ThermoFisher).

4.10. In vitro EV transmission imaging

The cells were treated with the BODIPY-labeled EVs derived from Colon26 or LuM1 at 11.5 μg/mL for 24 h. The cells were fixed with 4% paraformaldehyde in PBS (-) for 10 min and stained with ActinGreen488 (ThremoFisher) The nuclear counterstaining was performed using DAPI. Fluorescence images of random three fields (2,430 μm^2/field) were taken using a Floid® Imaging Station (ThermoFisher) and fluorescence-positive cells in each field were counted using ImageJ.

4.11. In vivo imaging

In vivo imaging experiments were performed in compliance with the guidelines of the Ethics Committee of Animal Care and Experimentation of Tokushima University (approval number T29-31). Eight weeks old female BALB/c mice (CLEA, Tokyo, Japan) were administered with 15 μg Cy7-labeled EVs per mouse by intraperitoneal injection. At 30 min after the injection, Cy7 fluorescence in the various organs of mice was analyzed by IVIS Spectrum imaging system.

4.12. Tumor allograft to mice

Animal experiments were performed according to the guidelines for care and use of laboratory animals approved by Okayama University (OKU-2018761) and the Japanese Pharmacological Society. Subcutaneous allograft was performed as previously described [6,21]. Colon26 cells (5.0×10^5 cells in 0.5 mL PBS) were transplanted subcutaneously into a side abdominal wall of each 6 to 7-week-old female BALB/c mice. Five micrograms per 0.5 mL (protein concentration) of EV fraction derived from Colon26 or LuM1, or 0.5 ml PBS was injected i.p. from Day 3 to 13, every other day, 6 times. On Day 21 after transplantation, the mice were sacrificed and subcutaneous tumors were measured each weight.

4.13. Cell proliferation

For analysis of cell proliferation, cells were seeded at a concentration of 2.5×10^3 cells/well in a 96-well plate. The number of cells at 1 to 5 days post-seeding period was counted by using Countess automated cell counter (ThermoFisher). The medium was replaced with fresh ones every 3 days during the analysis of cell proliferation.

4.14. Migration / Invasion assay

Migration and invasion assays were performed as previously described [21,59]. Uncoated and Matrigel-coated culture systems (Becton-Dickinson, Franklin Lakes, NJ) were used for in vitro migration and invasion assays, respectively. Cells were seeded at concentrations of 2.5×10^4 per well in a 24-well-plate into the upper chambers of transwells. Cells that migrated or invaded through the pores to the lower surface of the filter were fixed, stained using Diff-Quick stain (Sysmex, Kobe, Japan) and counted after 24 hours of the migration period.

4.15. Western blot analysis

Western blotting was performed as previously described [21,60]. Briefly, cells were lysed in a RIPA buffer (1% NP-40, 0.1% SDS, and 0.5% deoxycholate, and EDTA-free protease inhibitor cocktail in PBS) using 25-gauge syringes. The same protein amounts or the same number of cells were subjected to sodium dodecyl sulfate-polyacrylamide gel electrophoresis (SDS-PAGE), followed by transfer to a polyvinylidene fluoride (PVDF) membrane using wet- and semi-dry methods where appropriate. The membranes were blocked in 5% skim milk in Tris-buffered saline containing 0.05% Tween 20 for 60 min unless otherwise specified, incubated with a rabbit monoclonal anti-MMP3 antibody (EP1186Y, ab52915, Abcam) or a rabbit monoclonal anti-CD9 antibody (EPR2949, ab92726, Abcam). For CCN2/CTGF, blocking was performed in 10% skim milk overnight and a rabbit polyclonal anti-CCN2/CTGF antibody (ab6992, Abcam) was reacted for 2 days. The membranes were incubated with horseradish peroxidase (HRP)-conjugated secondary antibodies. For GAPDH, HRP-conjugated anti-GAPDH mouse monoclonal antibody (HRP-60004, Proteintech) was used. Blots were visualized with ECL substrate.

4.16. Microarray analysis and bioinformatics

Microarray analysis was performed as described [21,37]. Raw data was submitted to the Gene Expression Omnibus (GEO) database repository; accession ID: GSE97166; Colon26, GSM2553008; LuM1, GSM2553009; NM11, GSM2553010. Gene expression was analyzed using MeV 4.0 software (http://www.Tm4.org/mev.html) for the generation of heatmaps.

4.17. Real-time qRT-PCR

Preprints (www.preprints.org) | NOT PEER-REVIEWED | Posted: 19 February 2020 doi:10.20944/preprints202002.0281.v1

Peer-reviewed version available at Cancers 2020, 12, 881; doi:10.3390/cancers12040881

Total RNA preparation and qRT-PCR was carried out as described previously [21,61]. The miRNeasy mini kit (Qiagen) was used with DNase (Qiagen). The total RNA concentration was measured by using a micro spectrometer K2800 (Beijing Kaiao, Beijing, China). cDNA synthesis was carried out by using iScript™ cDNA Synthesis Kit (Bio-Rad). The primers are the blend of oligo (dT) and random primers. Specific primer pairs for *Mmp3, CCN2/CTGF,* and *Gapdh* (Table 5) were used for real-time PCR with iQ SYBR Green PCR mixture (Bio-Rad). Relative mRNA levels to *Gapdh* mRNA levels were quantified by the ΔΔCt method using the formula–fold change = $2^{-\Delta\Delta Ct}$. PCR reaction was carried out in triplicate and mean values were calculated with the mean ± S.D. of biological triplicates presented.

Table 5. The sequence of primers for RT-qPCR

Name of primers	5’ to 3’ sequences
m Gapdh Fw	ACCACAGTCCATGCCATCAC
m Gapdh Rv	TCCACCACCCTGTTGCTGTA
m Mmp3 Fw	ACCAACCTATTCCTGGTTGCTGCT
m Mmp3 Rv	ATGGAAACGGGACAAGTCTGTGGA
m CCN2/CTGF Fw	CTCCACCCGAGTTACCAATGACAA
m CCN2/CTGF Rv	CCAGAAAGCTCAAACTTGACAGGC

4.18. Patient-derived tumor samples

The co-expression correlation data set of colorectal adenocarcinoma with 632 patient-derived 632 samples (TCGA) was analyzed using cBioPortal.

4.19. Statistical analysis

Statistical significance was calculated using GraphPad Prism and Microsoft Excel. Three or more mean values were compared using one-way analysis of variance (ANOVA), while comparisons of 2 were done with an unpaired Student's *t*-test. $P < 0.05$ was considered to indicate statistical significance. Data were expressed as Mean ± SD unless otherwise specified.

Supplemental information

Fig. S1 | Full images of western blotting of MMP3 (A), CD9 (B), and GAPDH (C), supporting Fig. 1C.

Fig. S2 | Full images of western blotting of MMP3 (A) and GAPDH (B), supporting Fig. 1E.

Fig. S3 | Basic data of genome editing, supporting Fig. 3.

Fig. S4 | Full images of western blotting of CCN2/CTGF (A), CD9 (B), and GAPDH (C), supporting Fig. 4E.

Fig. S5 | Protein concentrations in each EV fraction derived from Colon26, LuM1, and MMP3-KO cells

Fig. S6 | Full images of western blotting of MMP3 (A) and GAPDH (B), supporting Fig. 6A.

Fig. S7 | Full images of western blotting of MMP3 (A), GAPDH (B), and CD9 (C), supporting Fig. 6A.

Fig. S8 | Full images of western blotting of MMP3 (A), CCN2/CTGF (B), and GAPDH (C), supporting Fig. 7A.

Acknowledgments

This paper is dedicated to the memory of one of our mentors, Professor Ken-ichi Kozaki, who passed away on May 29, 2016. The authors thank Yanyin Lu for illuminating discussion and technical assistance, Haruo Urata for the operation of TEM, and Kazuko Kobayashi for the operation of Zetasizer.

Funding

This work was supported by JSPS KAKENHI, grant numbers JP17K17895 (YO), JP17K11642 (TE), JP19H03817 (MT, TE), 19H04051 (HO, TE), JP17K11643 (CS, TE), 17K11669 (KOh, TE), 18K09789 (KN, TE), Ryobi Teien Memorial Foundation Grant (KOk, CS, TE), and by Suzuken Memorial Foundation (TE).

Author Contributions

YO performed animal experiments, genome editing, preparation of EVs, CLSM, western blotting, microarray, RT-qPCR, migration/invasion assays, coexpression correlation analysis, statistical analysis, acquired funding, and wrote an original draft of the manuscript. TE designed and managed the study, supervised YO, prepared materials, interpreted and visualized data, acquired fundings, edited and wrote the manuscript. MTT, EAT, and EA desined and performed western blotting. CS prepared EVs from cells, carried out luciferase assay and statistical analysis. KY and HO designed and performed in vivo imaging. MI performed EV transmission assay. KOn characterized EVs. KK prepared and maintained LuM1 cells, experimental protocols, and supervised TE, YO, and CS. SKC edited the manuscript. MT prepared resources, acquired funding, and edited the manuscript. KO supervised YO and TE. All authors reviewed the manuscript.

Conflicts of interest

The authors have no competing financial interests to declare.

Abbreviations:

CCN2, cellular communication network factor / CCN family 2

CIC, cancer-initiating cells

CLSM, confocal laser scanning microscopy

631 CSC, cancer stem cells

632 CTGF; Connective tissue growth factor

633 CRISPR; clustered regularly interspaced short palindromic repeat

634 ECM; extracellular matrix

635 EV; Extracellular vesicle

636 IVIS, in vivo imaging system

637 MMP; Moonlighting metalloproteinase

638 MV; Microvesicle

639 PEX; hemopexin-like repeat

References

1. Mueller, M.M.; Fusenig, N.E. Friends or foes – bipolar effects of the tumour stroma in cancer. *Nat Rev Cancer* **2004**, *4*, 839–849, doi:10.1038/nrc1477.
2. Ronald A. Ghossein, S.B.a.J.R. Molecular Detection of Micrometastases and Circulating Tumor Cells in Solid Tumors. *Clinical Cancer Research* **1999**, *5*.
3. Fujiwara, T.; Eguchi, T.; Sogawa, C.; Ono, K.; Murakami, J.; Ibaragi, S.; Asaumi, J.-i.; Calderwood, S.K.; Okamoto, K.; Kozaki, K.-i. Carcinogenic epithelial-mesenchymal transition initiated by oral cancer exosomes is inhibited by anti-EGFR antibody cetuximab. *Oral Oncology* **2018**, *86*, 251–257, doi:10.1016/j.oraloncology.2018.09.030.
4. Fujiwara, T.; Eguchi, T.; Sogawa, C.; Ono, K.; Murakami, J.; Ibaragi, S.; Asaumi, J.; Okamoto, K.; Calderwood, S.; Kozaki, K. Anti-EGFR antibody cetuximab is secreted by oral squamous cell carcinoma and alters EGF-driven mesenchymal transition. *Biochem Biophys Res Commun.* **2018**, *503*, 1267–1272.
5. Costa-Silva, B.; Aiello, N.M.; Ocean, A.J.; Singh, S.; Zhang, H.; Thakur, B.K.; Becker, A.; Hoshino, A.; Mark, M.T.; Molina, H., et al. Pancreatic cancer exosomes initiate pre-metastatic niche formation in the liver. *Nat Cell Biol* **2015**, *17*, 816–826, doi:10.1038/ncb3169.
6. Yokoi, A.; Yoshioka, Y.; Yamamoto, Y.; Ishikawa, M.; Ikeda, S.I.; Kato, T.; Kiyono, T.; Takeshita, F.; Kajiyama, H.; Kikkawa, F., et al. Malignant extracellular vesicles carrying MMP1 mRNA facilitate peritoneal dissemination in ovarian cancer. *Nat Commun* **2017**, *8*, 14470, doi:10.1038/ncomms14470.
7. Kong, J.; Tian, H.; Zhang, F.; Zhang, Z.; Li, J.; Liu, X.; Li, X.; Liu, J.; Li, X.; Jin, D., et al. Extracellular vesicles of carcinoma-associated fibroblasts creates a pre-metastatic niche in the lung through activating fibroblasts. *Mol Cancer* **2019**, *18*, 175, doi:10.1186/s12943-019-1101-4.
8. Peinado, H.; Aleckovic, M.; Lavotshkin, S.; Matei, I.; Costa-Silva, B.; Moreno-Bueno, G.; Hergueta-Redondo, M.; Williams, C.; Garcia-Santos, G.; Ghajar, C., et al. Melanoma exosomes educate bone marrow progenitor cells toward a pro-metastatic phenotype through MET. *Nat Med* **2012**, *18*, 883–891, doi:10.1038/nm.2753.
9. Al-Nedawi, K.; Meehan, B.; Micallef, J.; Lhotak, V.; May, L.; Guha, A.; Rak, J. Intercellular transfer of the oncogenic receptor EGFRvIII by microvesicles derived from tumour cells. *Nat Cell Biol* **2008**, *10*, 619–624, doi:10.1038/ncb1725.
10. Atay, S.; Wilkey, D.W.; Milhem, M.; Merchant, M.; Godwin, A.K. Insights into the Proteome of Gastrointestinal Stromal Tumors-Derived Exosomes Reveals New Potential Diagnostic Biomarkers. *Molecular & cellular proteomics : MCP* **2018**, *17*, 495–515, doi:10.1074/mcp.RA117.000267.
11. Taha, E.A.; Ono, K.; Eguchi, T. Roles of Extracellular HSPs as Biomarkers in Immune Surveillance and Immune Evasion. *Int J Mol Sci* **2019**, *20*, doi:10.3390/ijms20184588.

12. Eguchi, T.; Ono, K.; Kawata, K.; Okamoto, K.; Calderwood, S.K. Regulatory Roles of HSP90-Rich Extracellular Vesicles. In *Heat Shock Protein 90 in Human Diseases and Disorders*, Asea, A.A.A., Kaur, P., Eds. Springer Nature: 2019; pp. 3-17.
13. Ono, K.; Eguchi, T.; Sogawa, C.; Calderwood, S.K.; Futagawa, J.; Kasai, T.; Seno, M.; Okamoto, K.; Sasaki, A.; Kozaki, K.I. HSP-enriched properties of extracellular vesicles involve survival of metastatic oral cancer cells. *J Cell Biochem* **2018**, doi:10.1002/jcb.27039.
14. Eguchi, T.; Sogawa, C.; Okusha, Y.; Uchibe, K.; Iinuma, R.; Ono, K.; Nakano, K.; Murakami, J.; Itoh, M.; Arai, K., et al. Organoids with Cancer Stem Cell-like Properties Secrete Exosomes and HSP90 in a 3D NanoEnvironment. *PLOS ONE* **2018**, *13*, e0191109, doi:10.1371/journal.pone.0191109.
15. Erin, N.; Ogan, N.; Yerlikaya, A. Secretomes reveal several novel proteins as well as TGF-beta1 as the top upstream regulator of metastatic process in breast cancer. *Breast Cancer Res Treat* **2018**, *170*, 235-250, doi:10.1007/s10549-018-4752-8.
16. Gobin, E.; Bagwell, K.; Wagner, J.; Mysona, D.; Sandirasegarane, S.; Smith, N.; Bai, S.; Sharma, A.; Schleifer, R.; She, J.X. A pan-cancer perspective of matrix metalloproteases (MMP) gene expression profile and their diagnostic/prognostic potential. *BMC Cancer* **2019**, *19*, 581, doi:10.1186/s12885-019-5768-0.
17. Raja, U.M.; Gopal, G.; Shirley, S.; Ramakrishnan, A.S.; Rajkumar, T. Immunohistochemical expression and localization of cytokines/chemokines/growth factors in gastric cancer. *Cytokine* **2017**, *89*, 82-90, doi:10.1016/j.cyto.2016.08.032.
18. Mehner, C.; Miller, E.; Nassar, A.; Bamlet, W.R.; Radisky, E.S.; Radisky, D.C. Tumor cell expression of MMP3 as a prognostic factor for poor survival in pancreatic, pulmonary, and mammary carcinoma. *Genes Cancer* **2015**, *6*, 480-489, doi:10.18632/genesandcancer.90.
19. Wells, J.E.; Howlett, M.; Cole, C.H.; Kees, U.R. Deregulated expression of connective tissue growth factor (CTGF/CCN2) is linked to poor outcome in human cancer. *Int J Cancer* **2015**, *137*, 504-511, doi:10.1002/ijc.28972.
20. Kubota, S.; Takigawa, M. Cellular and molecular actions of CCN2/CTGF and its role under physiological and pathological conditions. *Clin Sci (Lond)* **2015**, *128*, 181-196, doi:10.1042/CS20140264.
21. Okusha, Y.; Eguchi, T.; Sogawa, C.; Okui, T.; Nakano, K.; Okamoto, K.; Kozaki, K.I. The intranuclear PEX domain of MMP involves proliferation, migration, and metastasis of aggressive adenocarcinoma cells. *J Cell Biochem* **2018**, *119*, 7363-7376, doi:10.1002/jcb.27040.
22. Radisky, D.C.; Levy, D.D.; Littlepage, L.E.; Liu, H.; Nelson, C.M.; Fata, J.E.; Leake, D.; Godden, E.L.; Albertson, D.G.; Nieto, M.A., et al. Rac1b and reactive oxygen species mediate MMP-3-induced EMT and genomic instability. *Nature* **2005**, *436*, 123-127, doi:10.1038/nature03688.

23. Shimo, T.; Kubota, S.; Yoshioka, N.; Ibaragi, S.; Isowa, S.; Eguchi, T.; Sasaki, A.; Takigawa, M. Pathogenic role of connective tissue growth factor (CTGF/CCN2) in osteolytic metastasis of breast cancer. *J Bone Miner Res* **2006**, *21*, 1045–1059, doi:10.1359/jbmr.060416.
24. Pu, N.; Gao, S.; Yin, H.; Li, J.A.; Wu, W.; Fang, Y.; Zhang, L.; Rong, Y.; Xu, X.; Wang, D., et al. Cell-intrinsic PD-1 promotes proliferation in pancreatic cancer by targeting CYR61/CTGF via the hippo pathway. *Cancer Lett* **2019**, *460*, 42–53, doi:10.1016/j.canlet.2019.06.013.
25. Kondo, S., Kubota, S., Shimo, T., Nishida, T., Yosimichi, G., Eguchi, T., ... & Takigawa, M. . Connective tissue growth factor increased by hypoxia may initiate angiogenesis in collaboration with matrix metalloproteinases. *Carcinogenesis* **2002**.
26. Eguchi, T.; Kubota, S.; Kawata, K.; Mukudai, Y.; Uehara, J.; Ohgawara, T.; Ibaragi, S.; Sasaki, A.; Kuboki, T.; Takigawa, M. Novel transcription-factor-like function of human matrix metalloproteinase 3 regulating the CTGF/CCN2 gene. *Mol Cell Biol* **2008**, *28*, 2391–2413, doi:10.1128/MCB.01288-07.
27. Eguchi, T.; Kubota, S.; Kawata K.; Mukudai Y.; Uehara J.; Ohgawara T.; Ibaragi S; Sasaki A.; Kuboki, T.; Takigawa, M. *Novel Transcriptional Regulation of CCN2/CTGF by Nuclear Translocation of MMP3*; Springer: Dordrecht, Nertherlands, 2010; pp. 255–264.
28. Hashimoto, G.; Inoki, I.; Fujii, Y.; Aoki, T.; Ikeda, E.; Okada, Y. Matrix metalloproteinases cleave connective tissue growth factor and reactivate angiogenic activity of vascular endothelial growth factor 165. *J Biol Chem* **2002**, *277*, 36288–36295, doi:10.1074/jbc.M201674200.
29. Kaasboll, O.J.; Gadicherla, A.K.; Wang, J.H.; Monsen, V.T.; Hagelin, E.M.V.; Dong, M.Q.; Attramadal, H. Connective tissue growth factor (CCN2) is a matricellular preproprotein controlled by proteolytic activation. *J Biol Chem* **2018**, *293*, 17953–17970, doi:10.1074/jbc.RA118.004559.
30. Eguchi, T.; Kubota, S.; Kondo, S.; Shimo, T.; Hattori, T.; Nakanishi, T.; Kuboki, T.; Yatani, H.; Takigawa, M. Regulatory mechanism of human connective tissue growth factor (CTGF/Hcs24) gene expression in a human chondrocytic cell line, HCS-2/8. *J Biochem* **2001**, *130*, 79–87.
31. Eguchi, T.; Kubota, S.; Kawata, K.; Mukudai, Y.; Ohgawara, T.; Miyazono, K.; Nakao, K.; Kondo, S.; Takigawa, M. Different transcriptional strategies for ccn2/ctgf gene induction between human chondrocytic and breast cancer cell lines. *Biochimie* **2007**, *89*, 278–288, doi:10.1016/j.biochi.2006.12.006.
32. Eguchi, T.; Kubota, S.; Kondo, S.; Kuboki, T.; Yatani, H.; Takigawa, M. A novel cis-element that enhances connective tissue growth factor gene expression in chondrocytic cells. *Biochem Biophys Res Commun* **2002**, *295*, 445–451.
33. Namba, Y.; Sogawa, C.; Okusha, Y.; Kawai, H.; Itagaki, M.; Ono, K.; Murakami, J.; Aoyama, E.; Ohyama, K.; Asaumi, J.I., et al. Depletion of Lipid Efflux Pump ABCG1 Triggers the Intracellular Accumulation of Extracellular Vesicles and Reduces Aggregation and

753 Tumorigenesis of Metastatic Cancer Cells. *Front Oncol* **2018**, *8*, 376,
754 doi:10.3389/fonc.2018.00376.
755 34. Sakata K; Kozaki K; Iida K; Tanaka R; Yamagata S; Utsumi KR; Saga S; Shimizu S; Matsuyama,
756 M. Establishment and characterization of high- and low-lung-metastatic cell lines derived
757 from murine colon adenocarcinoma 26 tumor line. *Jpn J Cancer Res (Cancer Sci)* **1996**, *87*,
758 78-85.
759 35. Munz, M.; Baeuerle, P.A.; Gires, O. The emerging role of EpCAM in cancer and stem cell
760 signaling. *Cancer Res* **2009**, *69*, 5627-5629, doi:10.1158/0008-5472.CAN-09-0654.
761 36. Oishi, N.; Yamashita, T.; Kaneko, S. Molecular biology of liver cancer stem cells. *Liver Cancer*
762 **2014**, *3*, 71-84, doi:10.1159/000343863.
763 37. Eguchi, T.; Calderwood, S.K.; Takigawa, M.; Kubota, S.; Kozaki, K.I. Intracellular MMP3
764 Promotes HSP Gene Expression in Collaboration With Chromobox Proteins. *J Cell Biochem*
765 **2017**, *118*, 43-51, doi:10.1002/jcb.25607.
766 38. You, Y.; Shan, Y.; Chen, J.; Yue, H.; You, B.; Shi, S.; Li, X.; Cao, X. Matrix metalloproteinase
767 13-containing exosomes promote nasopharyngeal carcinoma metastasis. *Cancer Sci* **2015**,
768 *106*, 1669-1677, doi:10.1111/cas.12818.
769 39. Dolo, V.; Ginestra, A.; Cassara, D.; Violini, S.; Lucania, G.; Torrisi, M.R.; Nagase, H.; Canevari,
770 S.; Pavan, A.; Vittorelli, M.L. Selective localization of matrix metalloproteinase 9, beta1
771 integrins, and human lymphocyte antigen class I molecules on membrane vesicles shed by
772 8701-BC breast carcinoma cells. *Cancer Res* **1998**, *58*, 4468-4474.
773 40. Ginestra, A.; Monea, S.; Seghezzi, G.; Dolo, V.; Nagase, H.; Mignatti, P.; Vittorelli, M.L.
774 Urokinase plasminogen activator and gelatinases are associated with membrane vesicles
775 shed by human HT1080 fibrosarcoma cells. *J Biol Chem* **1997**, *272*, 17216-17222,
776 doi:10.1074/jbc.272.27.17216.
777 41. Lai, R.C.; Tan, S.S.; Teh, B.J.; Sze, S.K.; Arslan, F.; de Kleijn, D.P.; Choo, A.; Lim, S.K.
778 Proteolytic Potential of the MSC Exosome Proteome: Implications for an Exosome-
779 Mediated Delivery of Therapeutic Proteasome. *Int J Proteomics* **2012**, *2012*, 971907,
780 doi:10.1155/2012/971907.
781 42. Wang, J.; Wu, Y.; Guo, J.; Fei, X.; Yu, L.; Ma, S. Adipocyte-derived exosomes promote lung
782 cancer metastasis by increasing MMP9 activity via transferring MMP3 to lung cancer cells.
783 *Oncotarget* **2017**, *8*, 81880-81891, doi:10.18632/oncotarget.18737.
784 43. Chowdhury, R.; Webber, J.P.; Gurney, M.; Mason, M.D.; Tabi, Z.; Clayton, A. Cancer exosomes
785 trigger mesenchymal stem cell differentiation into pro-angiogenic and pro-invasive
786 myofibroblasts. *Oncotarget* **2015**, *6*, 715-731, doi:10.18632/oncotarget.2711.
787 44. Hsieh, C.L.; Liu, C.M.; Chen, H.A.; Yang, S.T.; Shigemura, K.; Kitagawa, K.; Yamamichi, F.;
788 Fujisawa, M.; Liu, Y.R.; Lee, W.H., et al. Reactive oxygen species-mediated switching
789 expression of MMP-3 in stromal fibroblasts and cancer cells during prostate cancer
790 progression. *Sci Rep* **2017**, *7*, 9065, doi:10.1038/s41598-017-08835-9.

45. Wu, Y.L.; Li, H.Y.; Zhao, X.P.; Jiao, J.Y.; Tang, D.X.; Yan, L.J.; Wan, Q.; Pan, C.B. Mesenchymal stem cell-derived CCN2 promotes the proliferation, migration and invasion of human tongue squamous cell carcinoma cells. *Cancer Sci* **2017**, *108*, 897-909, doi:10.1111/cas.13202.
46. Makino, Y.; Hikita, H.; Kodama, T.; Shigekawa, M.; Yamada, R.; Sakamori, R.; Eguchi, H.; Morii, E.; Yokoi, H.; Mukoyama, M., et al. CTGF Mediates Tumor-Stroma Interactions between Hepatoma Cells and Hepatic Stellate Cells to Accelerate HCC Progression. *Cancer Res* **2018**, *78*, 4902-4914, doi:10.1158/0008-5472.Can-17-3844.
47. Ubink, I.; Verhaar, E.R.; Kranenburg, O.; Goldschmeding, R. A potential role for CCN2/CTGF in aggressive colorectal cancer. *J Cell Commun Signal* **2016**, *10*, 223-227, doi:10.1007/s12079-016-0347-5.
48. Zeitler, M.; Steringer, J.P.; Muller, H.M.; Mayer, M.P.; Nickel, W. HIV-Tat Protein Forms Phosphoinositide-dependent Membrane Pores Implicated in Unconventional Protein Secretion. *J Biol Chem* **2015**, *290*, 21976-21984, doi:10.1074/jbc.M115.667097.
49. Lonn, P.; Kacsinta, A.D.; Cui, X.S.; Hamil, A.S.; Kaulich, M.; Gogoi, K.; Dowdy, S.F. Enhancing Endosomal Escape for Intracellular Delivery of Macromolecular Biologic Therapeutics. *Sci Rep* **2016**, *6*, 32301, doi:10.1038/srep32301.
50. Staring, J.; Raaben, M.; Brummelkamp, T.R. Viral escape from endosomes and host detection at a glance. *J Cell Sci* **2018**, *131*, doi:10.1242/jcs.216259.
51. Shimo, T.; Nakanishi, T.; Nishida, T.; Asano, M.; Sasaki, A.; Kanyama, M.; Kuboki, T.; Matsumura, T.; Takigawa, M. Involvement of CTGF, a hypertrophic chondrocyte-specific gene product, in tumor angiogenesis. *Oncology* **2001**, *61*, 315-322, doi:10.1159/000055339.
52. Shimo, T.; Nakanishi, T.; Nishida, T.; Asano, M.; Kanyama, M.; Kuboki, T.; Tamatani, T.; Tezuka, K.; Takemura, M.; Matsumura, T., et al. Connective tissue growth factor induces the proliferation, migration, and tube formation of vascular endothelial cells in vitro, and angiogenesis in vivo. *J Biochem* **1999**, *126*, 137-145, doi:10.1093/oxfordjournals.jbchem.a022414.
53. Takigawa, M. The CCN Proteins: An Overview. *Methods Mol Biol* **2017**, *1489*, 1-8, doi:10.1007/978-1-4939-6430-7_1.
54. Shao, L.; Zhang, B.; Wang, L.; Wu, L.; Kan, Q.; Fan, K. MMP-9-cleaved osteopontin isoform mediates tumor immune escape by inducing expansion of myeloid-derived suppressor cells. *Biochem Biophys Res Commun* **2017**, *493*, 1478-1484, doi:10.1016/j.bbrc.2017.10.009.
55. Dezutter-Dambuyant, C.; Durand, I.; Alberti, L.; Bendriss-Vermare, N.; Valladeau-Guilemond, J.; Duc, A.; Magron, A.; Morel, A.P.; Sisirak, V.; Rodriguez, C., et al. A novel regulation of PD-1 ligands on mesenchymal stromal cells through MMP-mediated proteolytic cleavage. *Oncoimmunology* **2016**, *5*, e1091146, doi:10.1080/2162402x.2015.1091146.
56. Hyuga, S.; Nishikawa, Y.; Sakata, K.; Tanaka, H.; Yamagata, S.; Sugita, K.; Saga, S.; Matsuyama, M.; Shimizu, S. Autocrine factor enhancing the secretion of M(r) 95,000 gelatinase (matrix

metalloproteinase 9) in serum-free medium conditioned with murine metastatic colon carcinoma cells. *Cancer Res* **1994**, *54*, 3611-3616.

57. Tsuruo, T.; Yamori, T.; Naganuma, K.; Tsukagoshi, S.; Sakurai, Y. Characterization of metastatic clones derived from a metastatic variant of mouse colon adenocarcinoma 26. *Cancer Res* **1983**, *43*, 5437-5442.

58. Eguchi, T.; Kubota, S.; Takigawa, M. Promoter Analyses of CCN Genes. *Methods Mol Biol* **2017**, *1489*, 177-185, doi:10.1007/978-1-4939-6430-7_18.

59. Sogawa, C.; Eguchi, T.; Okusha, Y.; Ono, K.; Ohyama, K.; Iizuka, M.; Kawasaki, R.; Hamada, Y.; Takigawa, M.; Sogawa, N., et al. A reporter system evaluates tumorigenesis, metastasis, beta-catenin/MMP regulation, and druggability. *Tissue Eng Part A* **2019**, *25*, 1413-1425, doi:10.1089/ten.TEA.2018.0348.

60. Eguchi, T.; Prince, T.L.; Tran, M.T.; Sogawa, C.; Lang, B.J.; Calderwood, S.K. MZF1 and SCAND1 Reciprocally Regulate CDC37 Gene Expression in Prostate Cancer. *Cancers (Basel)* **2019**, *11*, doi:10.3390/cancers11060792.

61. Eguchi, T.; Watanabe, K.; Hara, E.S.; Ono, M.; Kuboki, T.; Calderwood, S.K. OstemiR: a novel panel of microRNA biomarkers in osteoblastic and osteocytic differentiation from mesencymal stem cells. *PLoS One* **2013**, *8*, e58796, doi:10.1371/journal.pone.0058796.

Preprints (www.preprints.org) | NOT PEER-REVIEWED | Posted: 19 February 2020 doi:10.20944/preprints202002.0281.v1

Peer-reviewed version available at Cancers 2020, 12, 881; doi:10.3390/cancers12040881

Supplementary information

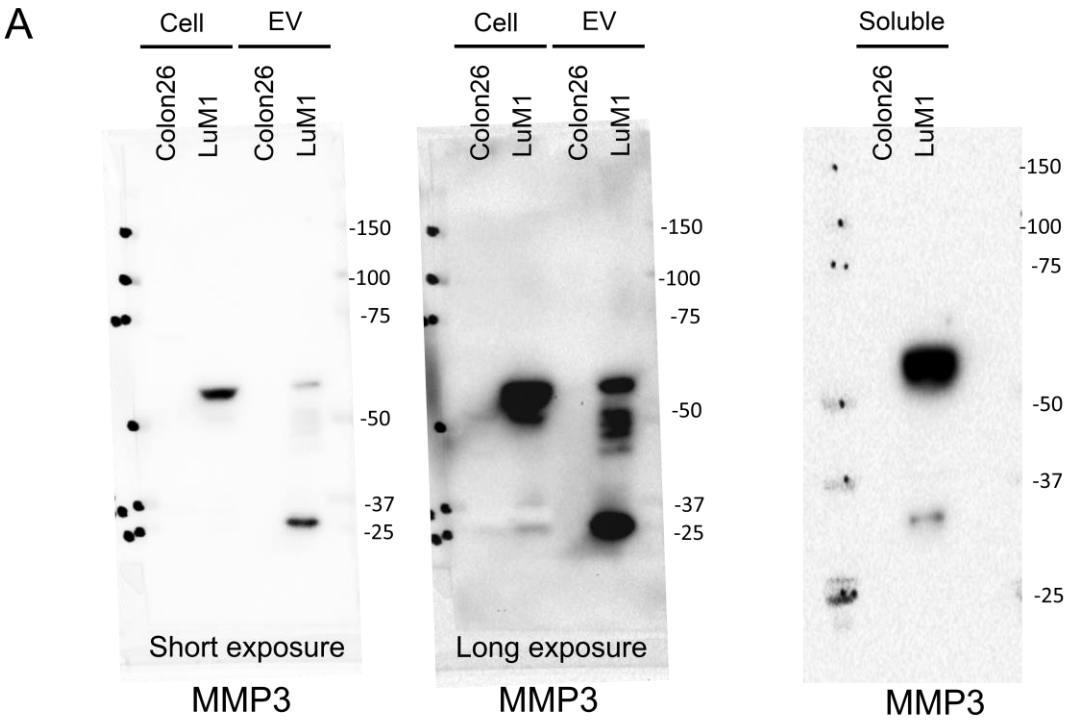

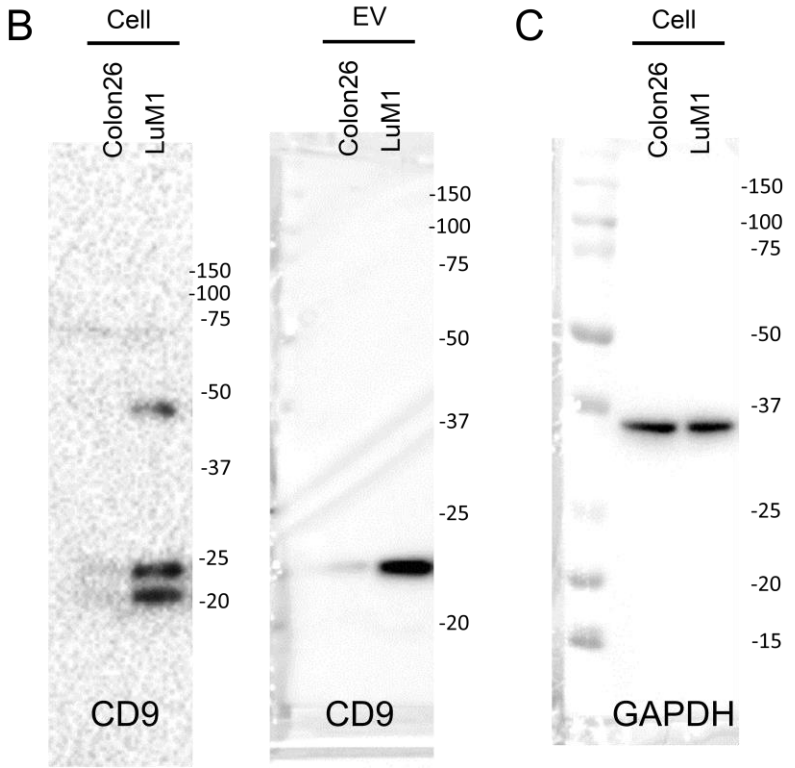

D

The number of applied cells	Cell lysate	EVs	Soluble
MMP3	$8.0x10^4$	$8.0x10^4$	$8.0x10^4$
CD9	$1.2x10^5$	$1.2x10^5$	-
GAPDH	$1.2x10^5$	-	-

Fig. S1 | Full images of western blotting of MMP3 (A), CD9 (B), and GAPDH (C), supporting Fig. 1C. The number of cells applied to each lane was shown in the panel D.

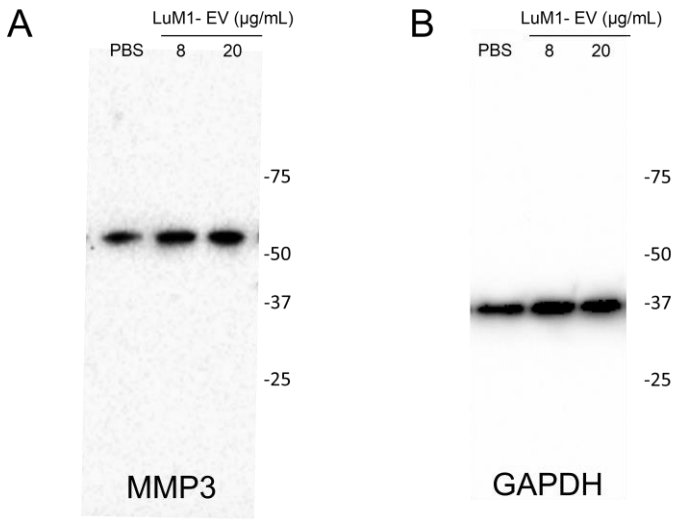

Fig. S2 | Full images of western blotting of MMP3 (A) and GAPDH (B), supporting Fig. 1E. To each well, 50 μg was applied.

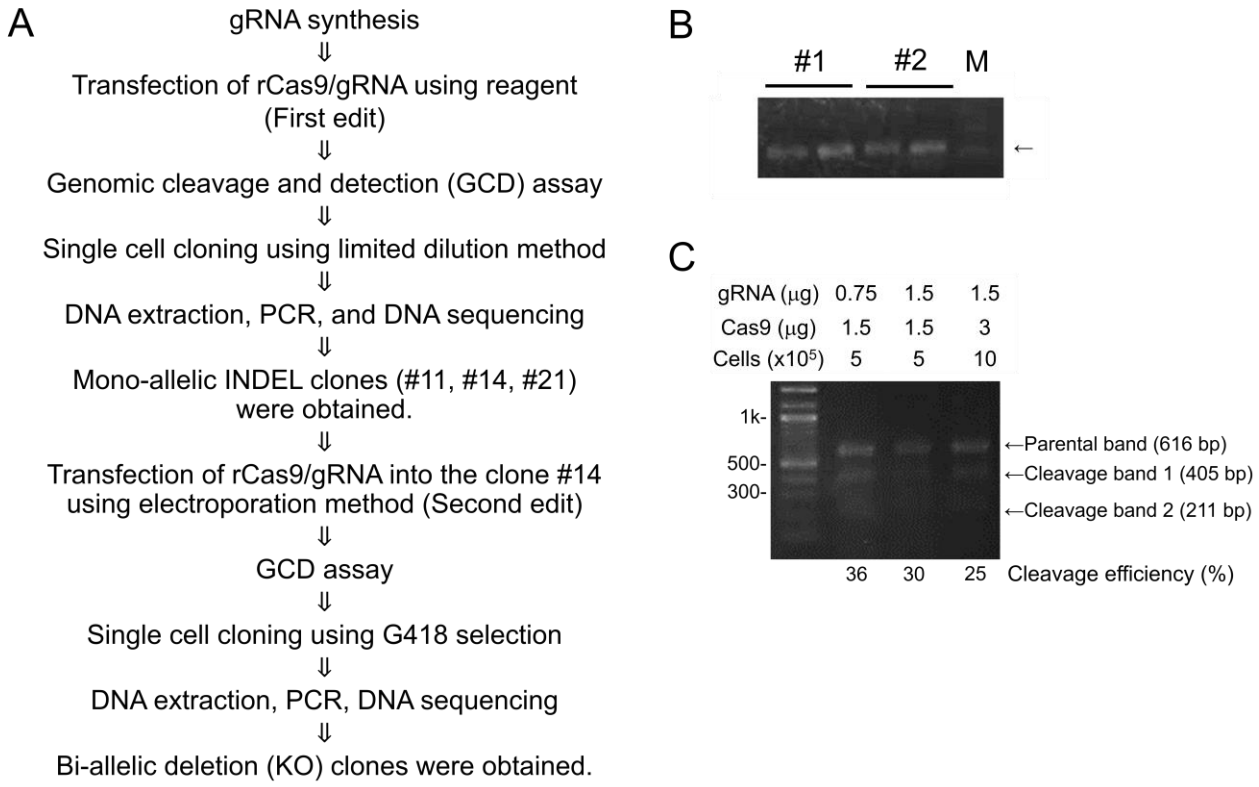

859 Fig. S3 | Basic data of genome editing, supporting Fig. 3. (A) A flow chart of genome editing. (B) Agarose gel
860 electrophoresis of the synthesized gRNA. #1, gRNA that targets exon 1 in mouse *Mmp3* gene, used in the
861 present study. #2, gRNA that targets exon 2 in mouse *Mmp3* gene, not used in the present study. M, molecular
862 weight marker. (C) Genome cleavage and detection (GCD) assay. The transfection conditions including the
863 amount of gRNA, Cas9, and cells were shown on the top. Genome cleavage efficiencies were shown on the
864 bottom. Parental band, cleavage band 1 and 2 were indicated by arrows.

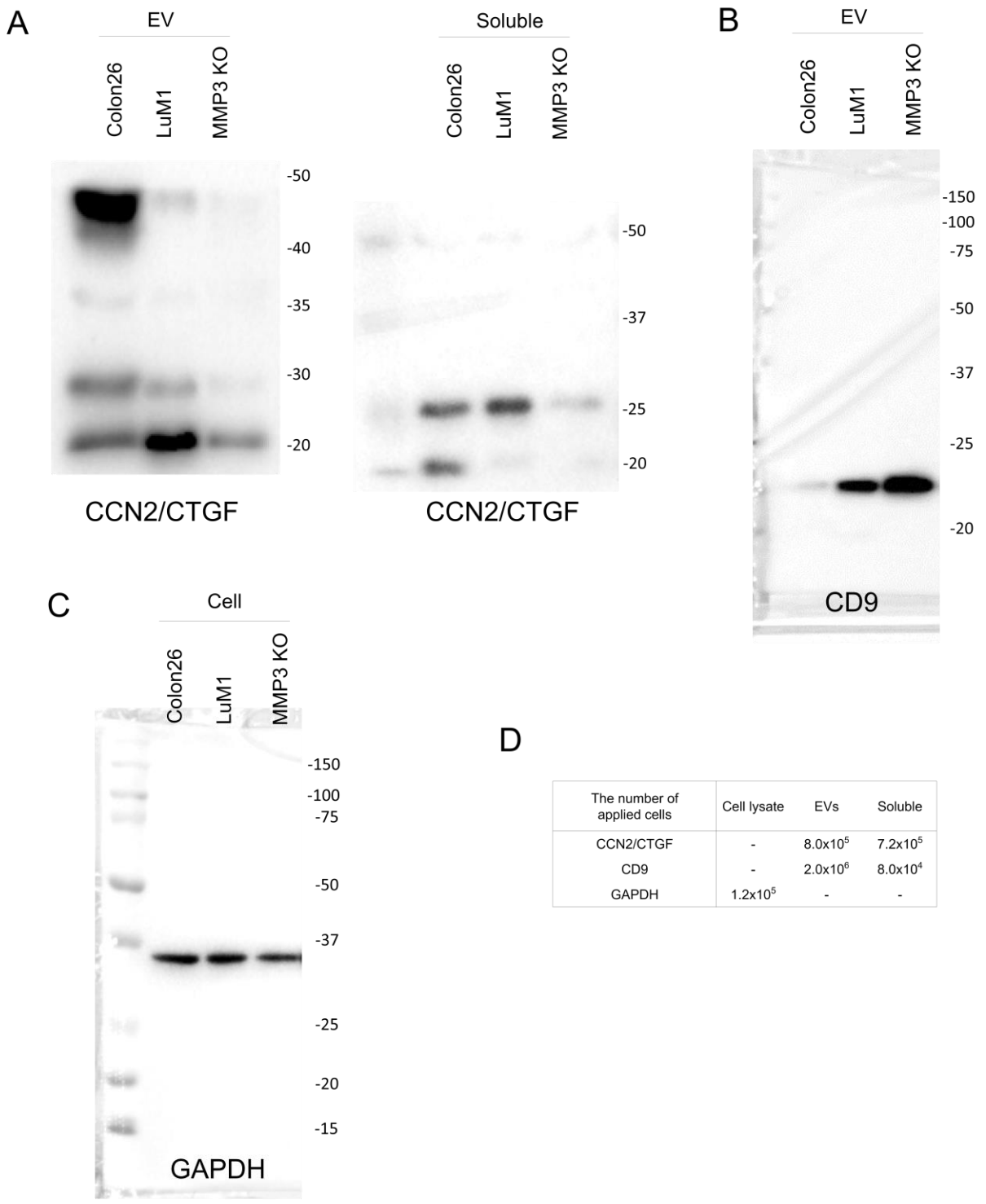

D

The number of applied cells	Cell lysate	EVs	Soluble
CCN2/CTGF	-	8.0×10^5	7.2×10^5
CD9	-	2.0×10^6	8.0×10^4
GAPDH	1.2×10^5	-	-

Fig. S4 | Full images of western blotting of CCN2/CTGF (A), CD9 (B), and GAPDH (C), supporting Fig. 4E. The number of cells applied to each lane was shown in the panel D.

Preprints (www.preprints.org) | NOT PEER-REVIEWED | Posted: 19 February 2020 doi:10.20944/preprints202002.0281.v1

Peer-reviewed version available at Cancers 2020, 12, 881; doi:10.3390/cancers12040881

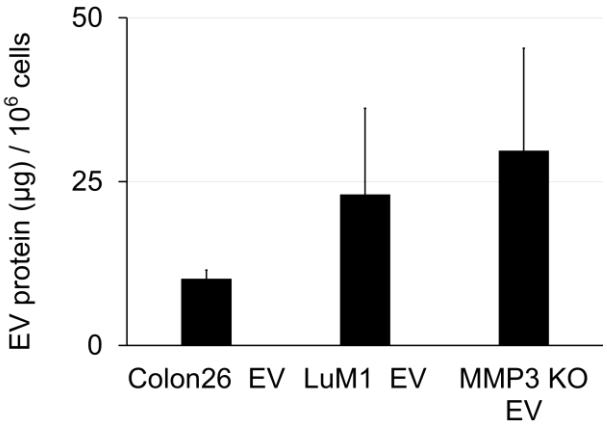

Fig. S5 | Protein concentrations in each EV fraction derived from Colon26, LuM1, and MMP3-KO cells

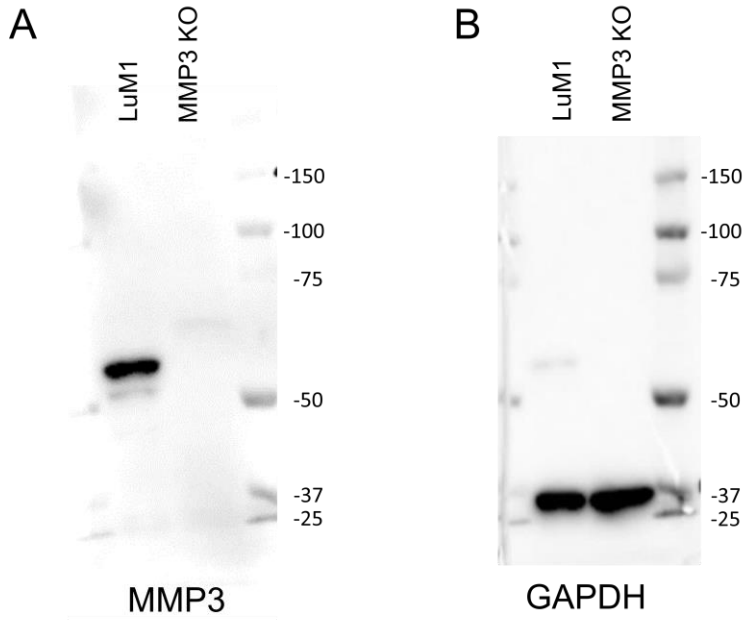

Fig. S6 | Full images of western blotting of MMP3 (A) and GAPDH (B), supporting Fig. 6A. To each well, 30 μg was applied.

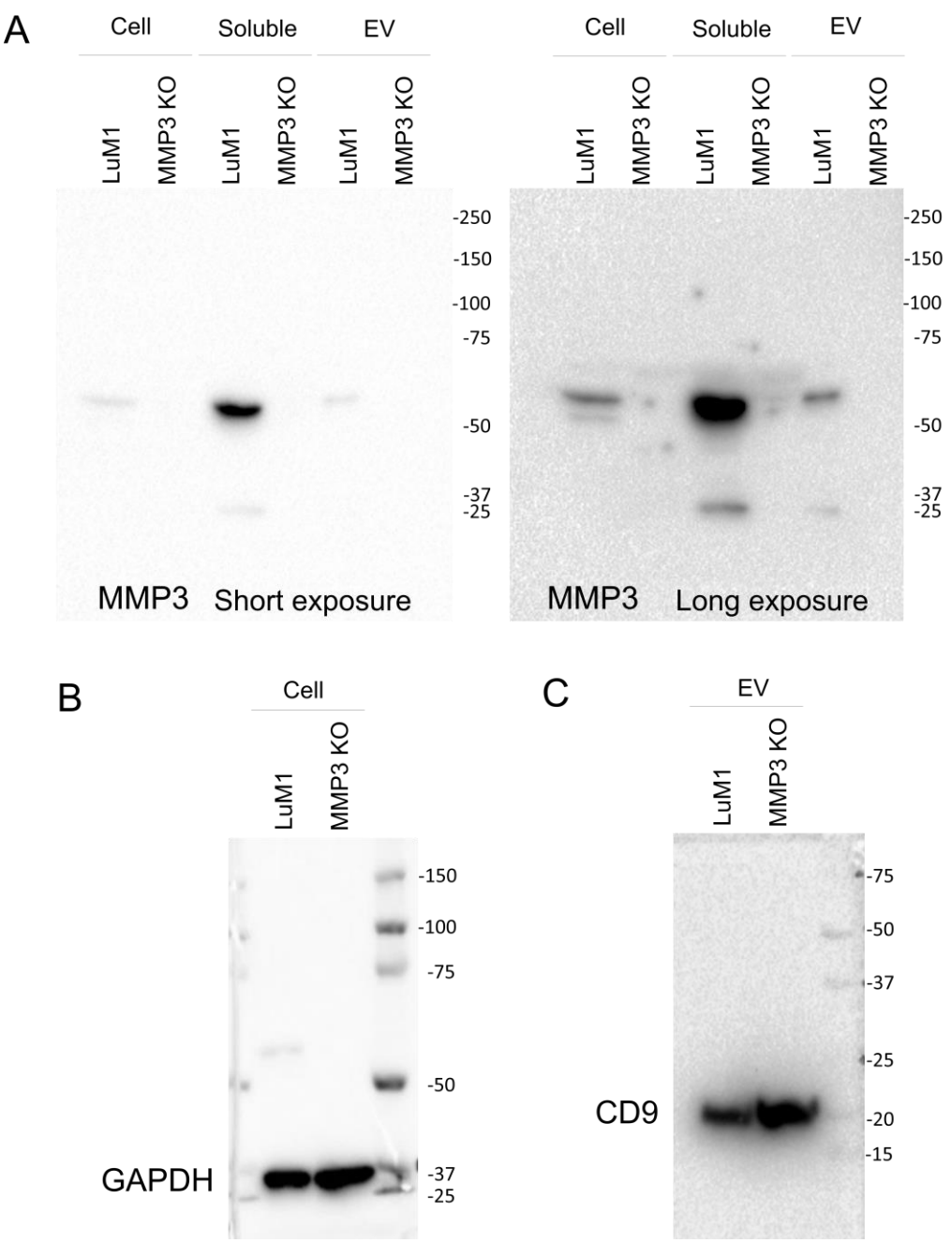

Fig. S7 | Full images of western blotting of MMP3 (A), GAPDH (B), and CD9 (C), supporting Fig. 6A. Protein samples prepared from 8.0 x 10^4 cells were applied to each lane.

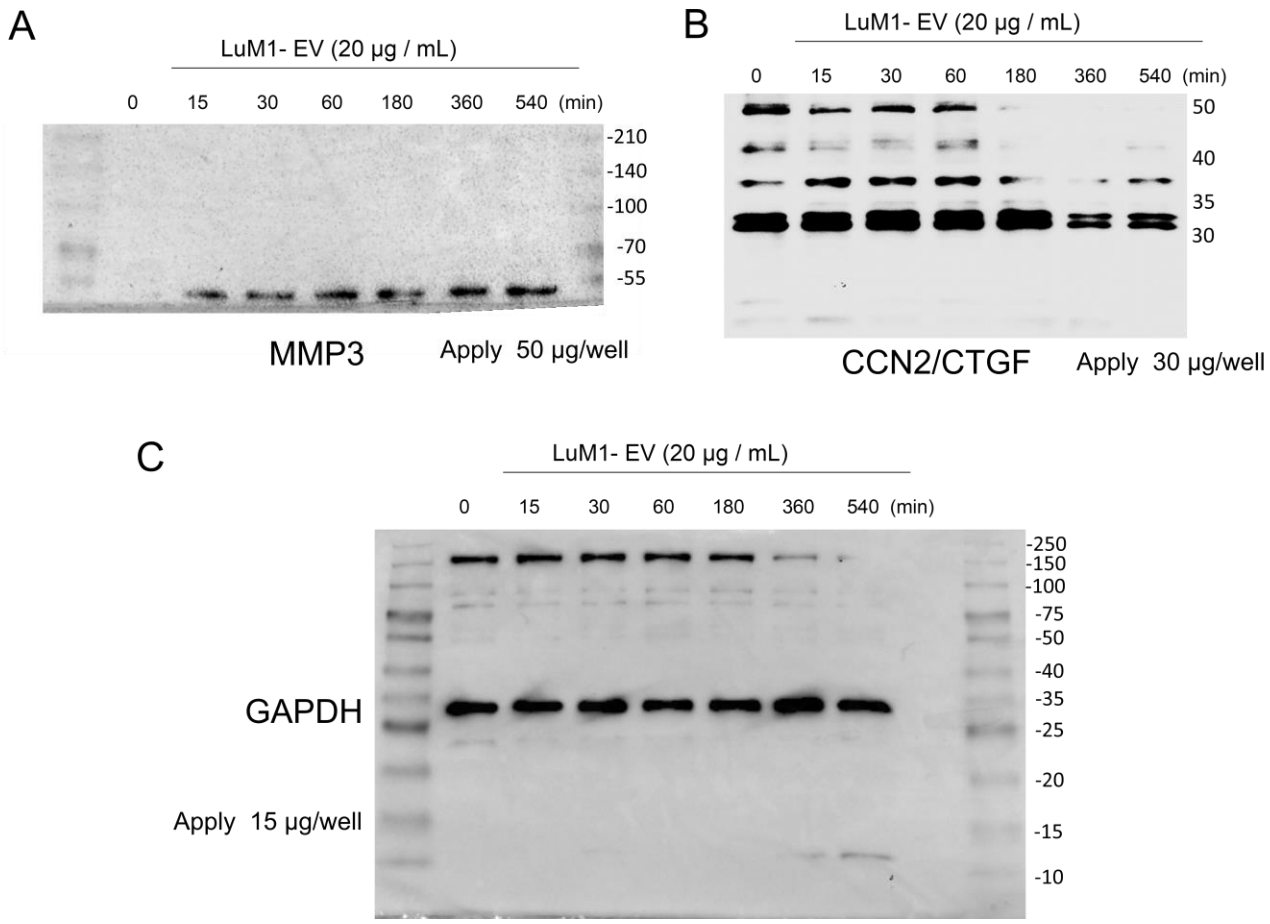

Fig. S8 | Full images of western blotting of MMP3 (A), CCN2/CTGF (B), and GAPDH (C), supporting Fig. 7A. (A) For MMP3, 50 µg protein sample was loaded to each lane; (B) 30 µg was loaded for CCN2/CTGF; (C) 15 µg was loaded for GAPDH.